Global fit to $b \to c\tau\nu$ anomalies as of Spring 2024

Syuhei Iguro,[1,2,3,4,5,*] Teppei Kitahara,[2,6,7,†] and Ryoutaro Watanabe[8,‡]

[1]*Institute for Advanced Research, Nagoya University, Nagoya 464–8601, Japan*
[2]*Kobayashi-Maskawa Institute for the Origin of Particles and the Universe, Nagoya University, Nagoya 464–8602, Japan*
[3]*KEK Theory Center, IPNS, KEK, Tsukuba 305–0801, Japan*
[4]*Institute for Theoretical Particle Physics (TTP), Karlsruhe Institute of Technology (KIT), Wolfgang-Gaede-Strasse 1, 76131 Karlsruhe, Germany*
[5]*Institute for Astroparticle Physics (IAP), Karlsruhe Institute of Technology (KIT), Hermann-von-Helmholtz-Platz 1, 76344 Eggenstein-Leopoldshafen, Germany*
[6]*Department of Physics, Graduate School of Science, Chiba University, Chiba 263–8522, Japan*
[7]*CAS Key Laboratory of Theoretical Physics, Institute of Theoretical Physics, Chinese Academy of Sciences, Beijing 100190, China*
[8]*Institute of Particle Physics and Key Laboratory of Quark and Lepton Physics (MOE), Central China Normal University, Wuhan, Hubei 430079, China*

(Received 8 April 2024; accepted 20 August 2024; published 9 October 2024)

Recently, several new experimental results of the test of lepton flavor universality (LFU) in $B \to D^{(*)}$ semileptonic decays were announced: the first result of R_D from the LHCb run 1 data, the first results of R_D and R_{D^*} from the LHCb run 2 data, and the first result of R_{D^*} from the Belle II collaboration. Including these new data, a global analysis still prefers the violation of the LFU between the tau and light leptons. A new world average of the data from the *BABAR*, LHCb, Belle, and Belle II collaborations is $R_D = 0.342 \pm 0.026$ and $R_{D^*} = 0.287 \pm 0.012$. Including this new data, we update a circumstance of the $b \to c\tau\bar{\nu}$ measurements and their implications for new physics (NP). Incorporating recent developments for the $B \to D^{(*)}$ form factors in the Standard Model, we observe a 4.4σ deviation from the Standard Model prediction. Our updates also include model-independent NP formulas for the related observables and the global fittings of parameters for leptoquark scenarios as well as single NP operator scenarios. Furthermore, we show future potential to indirectly distinguish different NP scenarios with the use of the precise measurements of the polarization observables in $B \to D^{(*)}\tau\bar{\nu}$ at the Belle II and the high-p_T flavored-tail searches at the LHC. We also discuss an impact on the LFU violation in $\Upsilon \to l^+l^-$.

DOI: 10.1103/PhysRevD.110.075005

I. INTRODUCTION

The semitauonic B-meson decays, $\bar{B} \to D^{(*)}\tau\bar{\nu}$, have been intriguing processes to measure the lepton flavor universality (LFU):

$$R_D \equiv \frac{\mathcal{B}(\bar{B} \to D\tau\bar{\nu}_\tau)}{\mathcal{B}(\bar{B} \to D\ell\bar{\nu}_\ell)}, \qquad R_{D^*} \equiv \frac{\mathcal{B}(\bar{B} \to D^*\tau\bar{\nu}_\tau)}{\mathcal{B}(\bar{B} \to D^*\ell\bar{\nu}_\ell)}, \quad (1.1)$$

since it has been reported that the global average of the measurements by the *BABAR* [1,2], LHCb from run 1 and run 2 data [3–6], Belle [7–11], and recently Belle II collaborations [12,13] indicates a deviation from the Standard Model (SM) prediction. Here, $\ell = e, \mu$ for the *BABAR*/Belle/Belle II, while $\ell = \mu$ for the LHCb collaborations. See Table I for the present experimental summary with including the HFLAV collaboration's preliminary average in the spring of 2024 [14].

A key feature of this deviation is that the world average of the measured values of R_D and R_{D^*} significantly exceeds their SM predictions and thus implies violation of the LFU between the tau and light leptons. Then it has been followed by a ton of theoretical studies to understand its implication from various points of view, e.g., see Refs. [20,21] and references therein. A confirmation of the LFU violation will provide evidence of new physics (NP).

*Contact author: igurosyuhei@gmail.com
†Contact author: kitahara@chiba-u.jp
‡Contact author: watanabe@ccnu.edu.cn

TABLE I. Current status of the independent experimental R_{D^*} and R_D measurements. The first and second errors are statistical and systematic, respectively.

Experiment	R_{D^*}	R_D	Correlation
BABAR [1,2]	$0.332 \pm 0.024 \pm 0.018$	$0.440 \pm 0.058 \pm 0.042$	−0.27
Belle [7]	$0.293 \pm 0.038 \pm 0.015$	$0.375 \pm 0.064 \pm 0.026$	−0.49
Belle [8,9]	$0.270 \pm 0.035^{+0.028}_{-0.025}$	...	...
Belle [10,11]	$0.283 \pm 0.018 \pm 0.014$	$0.307 \pm 0.037 \pm 0.016$	−0.51
LHCb [3,6,15]	$0.281 \pm 0.018 \pm 0.024$	$0.441 \pm 0.060 \pm 0.066$	−0.43
LHCb [4,5,16,17]	$0.267 \pm 0.012 \pm 0.019$	...	...
Belle II [13,18]	$0.262^{+0.041+0.035}_{-0.039-0.032}$	...	...
LHCb [19]	$0.402 \pm 0.081 \pm 0.085$	$0.249 \pm 0.043 \pm 0.047$	−0.39
World average [14]	0.287 ± 0.012	0.342 ± 0.026	−0.39

A. Summary of the current status: Spring 2024

The LHCb collaboration showed their results of R_{D^*} with a semileptonic-tagging method ($\tau \to \mu\bar{\nu}\nu$) in 2015 [3] and a hadronic-tagging method ($\tau \to 3\pi\nu$) in 2017 [4,5] using the LHCb run 1 dataset. At the end of 2022 [15], they reported the first results of R_D as well as R_{D^*} with the semileptonic tagging method using the LHCb run 1 dataset [6],

$$R_D^{\mathrm{LHCb2022}} = 0.441 \pm 0.060_{\mathrm{stat}} \pm 0.066_{\mathrm{syst}},$$
$$R_{D^*}^{\mathrm{LHCb2022}} = 0.281 \pm 0.018_{\mathrm{stat}} \pm 0.024_{\mathrm{syst}}. \quad (1.2)$$

This result superseded the previous result reported in 2015. Furthermore, in early 2023 [16], they reported the first result of R_{D^*} with the hadronic-tagging method using the combined dataset of the LHCb run 1 and part of the run 2 [17],

$$R_{D^*}^{\mathrm{LHCb2023}} = 0.267 \pm 0.012_{\mathrm{stat}} \pm 0.019_{\mathrm{syst}}, \quad (1.3)$$

which superseded the previous result in 2017.

In addition, in March 2024 the LHCb collaboration announced preliminary results of R_D and R_{D^*} with the semileptonic-tagging method using the partial run 2 dataset [19],

$$R_D^{\mathrm{LHCb2024}} = 0.249 \pm 0.043_{\mathrm{stat}} \pm 0.047_{\mathrm{syst}},$$
$$R_{D^*}^{\mathrm{LHCb2024}} = 0.402 \pm 0.081_{\mathrm{stat}} \pm 0.085_{\mathrm{syst}}. \quad (1.4)$$

The uncertainty of $R_{D^*}^{\mathrm{LHCb2024}}$ is large, while the one of R_D^{LHCb2024} is small enough to push the world average down.

In the meantime, at last, the Belle II collaboration has started their data taking from 2019 [12]. Recently, they reported a first preliminary result of R_{D^*} with a semileptonic tagging method ($\tau \to \ell\bar{\nu}\nu$) [13,18]:

$$R_{D^*}^{\mathrm{BelleII}} = 0.262^{+0.041}_{-0.039\mathrm{stat}}{}^{+0.035}_{-0.032\mathrm{syst}}. \quad (1.5)$$

The experimental uncertainty of the Belle II result is still large. However, the amount of the integrated luminosity used in the Belle II analysis (189 fb^{-1}) is only a quarter of one of the Belle (711 fb^{-1}). Therefore, it is expected that this uncertainty will be reduced significantly in the near future [22].

Moreover, the CMS collaboration has developed an innovative data recording method, called "*B* Parking" since 2019 [23–26]. Although their official first results for $R_{D^{(*)}}$ are still being awaited, it would be expected that the size of the experimental uncertainty is comparable to the other *B* factories.

In Table I, we summarize the current status of the $R_{D^{(*)}}$ measurements including the new LHCb and Belle II results. It is found that the above four new results are consistent with the previous world average evaluated by the HFLAV collaboration in 2021 [27], whose p value is 28% with $\chi^2/\mathrm{d.o.f.} = 8.8/7$. Including all available data in Table I, the preliminary world averages of $R_{D^{(*)}}$ were evaluated by the HFLAV [14] as

$$R_D = 0.342 \pm 0.026,$$
$$R_{D^*} = 0.287 \pm 0.012, \quad (1.6)$$

with the R_D–R_{D^*} correlation of −0.39. It gives the p value among all data as 35% with $\chi^2/\mathrm{d.o.f.} = 12.11/11$.

Regarding the combined average, an important analysis is given in Ref. [28]. The authors pointed out that evaluations of the D^{**} distributions in the SM background involve nontrivial correlations that affect the $R_{D^{(*)}}$ measurements. Their sophisticated study shows that the combined $R_{D^{(*)}}$ average is slightly sifted, which is beyond the scope of our work since the size of the shift depends on the details of the experimental setup.

Recent SM predictions for $R_{D^{(*)}}^{\mathrm{SM}}$ have been obtained in Refs. [14,29–32] as summarized in Table II. The differences in these SM predictions are mainly due to the development of the $\bar{B} \to D^{(*)}$ form factor evaluations both by theoretical studies and experimental fits. For the moment, the HFLAV takes the "arithmetic" average [14] for the SM prediction based on the seven representative works [31,33–38], in which several form-factor

TABLE II. Summary of the SM predictions for the $\bar{B} \to D^{(*)}\tau\bar{\nu}$ and related observables. The current averaged values of the experimental measurements are also written in the last row. See the main text for explanations of differences between the SM predictions.

Reference	R_D	R_{D^*}	P_τ^D	$-P_\tau^{D^*}$	$F_L^{D^*}$	$R_{J/\psi}$	R_{Λ_c}	$R_{\Upsilon(3S)}$
Bernlochner *et al.* [29]	0.288(4)	0.249(3)	⋯	⋯	⋯	⋯	⋯	⋯
Iguro and Watanabe [30]	0.290(3)	0.248(1)	0.331(4)	0.497(7)	0.464(3)	⋯	⋯	⋯
Bordone *et al.* [31,32]	0.298(3)	0.250(3)	0.321(3)	0.492(13)	0.467(9)	⋯	⋯	⋯
HFLAV2024 [14]	0.298(4)	0.254(5)	⋯	⋯	⋯	⋯	⋯	⋯
References [43–45]	⋯	⋯	⋯	⋯	⋯	0.258(4)	0.324(4)	0.9948
Data	0.342(26)	0.287(12)	⋯	$0.38^{+0.53}_{-0.55}$	0.49(5)	0.61(18)	0.271(72)	0.968(16)

parametrizations are used for their fit analyses. The important notices of these references are (i) the Caprini-Lellouch-Neubert (CLN) parametrization is no longer adopted and (ii) the recent lattice studies [39–41] for $B \to D^*$ transition are not included. In Table II, we refer to Refs. [31,32] separately from the HFLAV average since it obtains the distinct $R_{D^*}^{\rm SM}$. This study has considered the heavy quark effective theory (HQET) corrections up to $\mathcal{O}(\alpha_s, \Lambda_{\rm QCD}/m_b, \Lambda_{\rm QCD}^2/m_c^2)$, and utilized the approximate $SU(3)_F$ relation to the $\bar{B}_s \to D_s^{(*)}$ form factors that have been determined by the HPQCD lattice result [42]. Reference [30] also takes the same HQET form factor as above but includes the $B \to D^{(*)}\ell\nu$ differential angular distribution data for the fit, which is distinct from the former study. For comparison, we also refer to the recent study of Ref. [29] that has included the $B \to D^*$ lattice study by Fermilab-MILC (FM) [39]. In this work, we will employ the work of Ref. [30] for the form factor evaluations as explained later.

A further concern for the SM evaluation is long-distance QED corrections to $\bar{B} \to D^{(*)}\ell\bar{\nu}$, which remains an open question. They depend on the lepton mass as being of $\mathcal{O}[\alpha \ln(m_\ell/m_B)]$ and hence it could provide a few percent corrections to violation of the LFU in the semileptonic processes [46–49]. This will be crucial in the future when the LHCb and Belle II experiments reach such an accuracy.

In Fig. 1, we show the latest average of the R_D–R_{D^*} along with the several recent SM predictions. A general consensus from the figure is that the deviation of the experimental data from the SM expectations still remains. For instance, applying the SM prediction from {HFLAV2024 [14], Bernlochner *et al.* [29], Iguro-Watanabe [30], Bordone *et al.* [31,32]}, one can see $\{3.3\sigma, 4.2\sigma, 4.4\sigma, 3.9\sigma\}$ deviations corresponding to p-value $= \{8.9 \times 10^{-4}, 2.3 \times 10^{-5}, 1.1 \times 10^{-5}, 1.2 \times 10^{-4}\}$ ($\Delta\chi^2 = \{14.0, 21.4, 22.8, 18.1\}$ for two degrees of freedom), respectively.

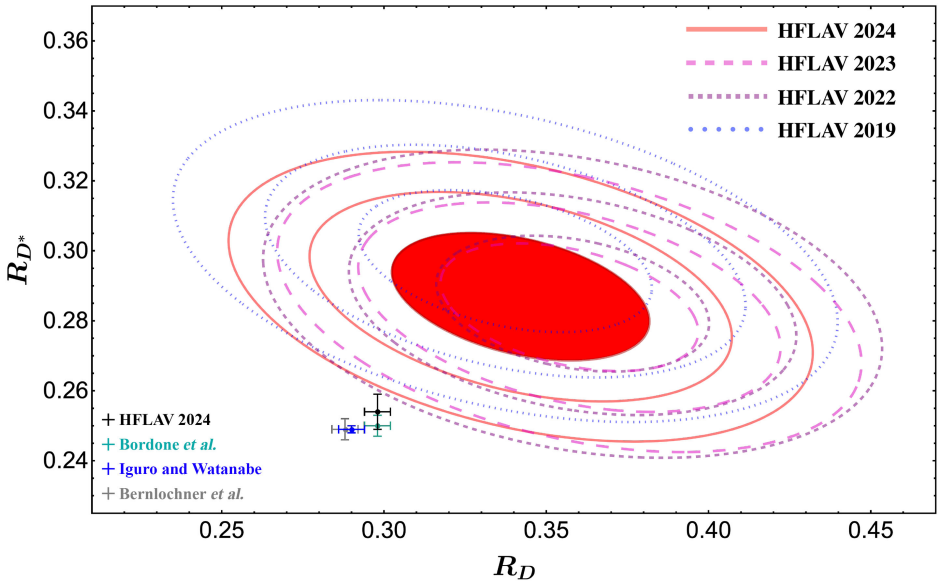

FIG. 1. The world average of the latest R_D and R_{D^*} experimental results by HFLAV 2024 (1, 2, 3σ red-solid contours). The former world averages are also shown: the HFLAV 2023, 2022 and 2019 averages by long-dashed, dashed and dotted contours, respectively. On the other hand, the several SM predictions are shown by crosses [14,29–32] (see also Table II).

In addition to these deviations in the LFU measurements, τ- and D^*-polarization observables in $\bar{B} \to D^{(*)}\tau\bar{\nu}$ also provide us important and nontrivial information. This is because these observables can potentially help us to pin down the NP structure that causes these deviations [50–67]. We refer to the τ longitudinal-polarization asymmetry in $\bar{B} \to D^{(*)}\tau\bar{\nu}$ and the fraction of the D^*-longitudinal mode in $\bar{B} \to D^*\tau\bar{\nu}$ as $P_\tau^{D^{(*)}}$ and $F_L^{D^*}$, respectively. See Refs. [59,68,69] for their explicit definitions.

In recent years, the first measurements for some of the above polarization observables have been reported by the Belle collaboration. It is summarized as $P_\tau^{D^*\mathrm{Belle}} = -0.38 \pm 0.51_{\mathrm{stat}}{}^{+0.21}_{-0.16\mathrm{syst}}$ [8] and $F_L^{D^*\mathrm{Belle}} = 0.60 \pm 0.08_{\mathrm{stat}} \pm 0.04_{\mathrm{syst}}$ [70]. Note that the latter is still a preliminary result. More recently, the LHCb collaboration reported the first preliminary result of $F_L^{D^*}$ using the combined dataset of the LHCb run 1 and part of the run 2; $F_L^{D^*,\mathrm{LHCb}} = 0.43 \pm 0.06_{\mathrm{stat}} \pm 0.03_{\mathrm{syst}}$ [71,72]. Naively combining these results, we obtain the average value as

$$F_L^{D^*} = 0.49 \pm 0.05, \tag{1.7}$$

which is well consistent with the SM prediction, see Table II. Note that although P_τ^D is the most striking observable to disentangle the leptoquark (LQ) scenarios that can explain the anomalies, the experimental result does not exist so far.

Furthermore, the D^*-longitudinal polarization in the electron and muon modes have been measured very precisely by the full Belle data set $F_{L,\mathrm{Belle}}^{D^*,e} = 0.485 \pm 0.017_{\mathrm{stat}} \pm 0.005_{\mathrm{sys}}$ and $F_{L,\mathrm{Belle}}^{D^*,\mu} = 0.518 \pm 0.017_{\mathrm{stat}} \pm 0.005_{\mathrm{sys}}$ [73], and also the first Belle II data $F_{L,\mathrm{BelleII}}^{D^*,e} = 0.520 \pm 0.005_{\mathrm{stat}} \pm 0.005_{\mathrm{sys}}$ and $F_{L,\mathrm{BelleII}}^{D^*,\mu} = 0.527 \pm 0.005_{\mathrm{stat}} \pm 0.005_{\mathrm{sys}}$ [74]. We obtain the naive averaged value,

$$\begin{aligned} F_L^{D^*,e} &= 0.515 \pm 0.007, \\ F_L^{D^*,\mu} &= 0.526 \pm 0.007. \end{aligned} \tag{1.8}$$

They are also consistent with the SM predictions, $F_{L,\mathrm{SM}}^{D^*,\ell}(\ell = e,\mu) = 0.534 \pm 0.002$ [30,75] (to be exact, there is a 2.7σ level tension in $F_L^{D^*,e}$).

Besides the first direct measurement of the LFU test for the inclusive mode, $R_X \equiv \mathcal{B}(\bar{B} \to X\tau\bar{\nu}_\tau)/\mathcal{B}(\bar{B} \to X\ell\bar{\nu}_\ell)$, has been performed by the Belle II collaboration. Here, X indicates any hadronic final states coming from $b \to c l\bar{\nu}$ and $b \to u l\bar{\nu}$ processes. A robust correlation is expected between R_X and $R_{D^{(*)}}$ because the inclusive mode is dominated by the exclusive D and D^* modes. Recently, the Belle II collaboration reported the preliminary result, $R_X = 0.228 \pm 0.016_{\mathrm{stat}} \pm 0.036_{\mathrm{syst}}$ [76,77]. This result is not only consistent with the SM prediction $R_X^{\mathrm{SM}} = 0.223 \pm 0.005$ [78–80] but also consistent with the $R_{D^{(*)}}$ anomalies [77]. Note that based on the LEP data of $\mathcal{B}(b \to X\tau\bar{\nu}_\tau)$ [81] and assuming that each individual b hadron has the same width, $R_{X_c} = 0.223 \pm 0.030$ has been estimated [82,83], which is consistent with the Belle II result. See Ref. [83] for a detailed NP analysis of R_{X_c}.

B. Preliminaries of our analysis

The main points of this paper are that (i) we provide state-of-the-art numerical NP formulas for the observables relevant to the semitauonic B decays and (ii) we revisit to perform global fits to the available $R_{D^{(*)}}$ measurements with respect to NP interpretations. It will be given by incorporating the following updates and concerns:

(1) Three new results of the LFU test from the LHCb collaboration ($R_{D^{(*)}}^{\mathrm{LHCb2022}}$, $R_{D^*}^{\mathrm{LHCb2023}}$, and $R_{D^{(*)}}^{\mathrm{LHCb2024}}$) and the preliminary result from the Belle II collaboration ($R_{D^*}^{\mathrm{BelleII}}$) are encoded in our global analysis as shown in Table I.

(2) The preliminary result of the D^*-polarization fraction from the LHCb collaboration ($F_L^{D^*,\mathrm{LHCb}}$) is encoded in our global analysis as shown in Table I.

(3) The recent development of the $\bar{B} \to D^{(*)}$ transition form factors is taken into account, which is summarized in the previous section. It is described by the HQET taking higher-order corrections up to $\mathcal{O}(\Lambda_{\mathrm{QCD}}^2/m_c^2)$ as introduced in Refs. [29,31,84]. We follow the result from the comprehensive theory + experiment fit analysis as obtained in Ref. [30].[1]

(4) A recent study introduced an approximation method to reduce independent parameters involving the $\mathcal{O}(\Lambda_{\mathrm{QCD}}^2/m_c^2)$ corrections in HQET [29]. Although this affects some of the parameter fits for the form factors, our reference values of $R_{D^{(*)}}^{\mathrm{SM}}$ from Ref. [30] are consistent with those of Ref. [29], shown in Table II. Hence, we do not take this approximation in the present work.

(5) The FM collaborations [39] presented the first lattice result of the form factors for $\bar{B} \to D^*\ell\bar{\nu}$ at the nonzero recoil points. The FM result with the light-lepton experimental data predicts $R_{D^*}^{\mathrm{SM}} = 0.2484 \pm 0.0013$, which is consistent with our reference value of Ref. [30]. Currently, JLQCD [40] and HPQCD [41] collaborations presented preliminary results at the nonzero recoil points. Since their results need to be finalized and compared with each other, we do not include these lattice updates in the present work. See Refs. [85,86] for the recent theoretical studies based on these lattice results.

[1]To be precise, we employ the "(2/1/0) fit" result, preferred by their fit analysis. See the reference for details.

(6) The dispersive matrix method can determine the form factors based on only the lattice data with the unitary bound, which is free from the parametrization method [38,87,88]. Even though the lattice uncertainties are still large, this method predicts $R_D^{\rm SM} = 0.296 \pm 0.008$ [88] and $R_{D^*}^{\rm SM} = 0.262 \pm 0.009$ [85] (including above lattice results at the nonzero recoil), which are consistent with the world averages of $R_{D^{(*)}}$ in Eq. (1.6) and also the SM predictions of Ref. [30] with less than 2σ level. However, it has been recently pointed out that this method provides an additional tension in $F_L^{D^*,\ell}(\ell = e,\mu)$ at 2.4σ level [75,85]. In the present work, we do not employ this method.

(7) Indirect LHC bounds from the high-p_T mono-τ searches with large missing transverse energy [89–99] are concerned. We impose the result of Ref. [97] that directly constrains the NP contributions to the $b \to c\tau\bar{\nu}$ current and accounts for the NP-scale dependence on the LHC bound, which is not available in the effective-field-theory description. Requiring an additional b-tagged jet also helps to improve the sensitivity [96,98]. We will see how it affects the constraints in the LQ scenarios.

(8) Similar sensitivity can be obtained by the $\tau^+\tau^-$ final state [100,101]. It is noted that about three standard deviations are reported by the CMS collaboration [101], which would imply the existence of leptoquark, while the ATLAS result [100] has not found a similar excess. We need the larger statistics to confirm it, and, thus, we do not include the constraint to be conservative.

In addition to the above points, we also investigate the following processes that are directly/indirectly related to the $b \to c\tau\bar{\nu}$ current:

(1) The LFU in $B_c \to J/\psi l\bar{\nu}$ decays is connected to $R_{D^{(*)}}$ through the same $b \to cl\bar{\nu}$ currents. The LHCb collaboration has measured the ratio $R_{J/\psi}^{\rm LHCb} \equiv \mathcal{B}(B_c \to J/\psi\tau\bar{\nu})/\mathcal{B}(B_c \to J/\psi\mu\bar{\nu}) = 0.71 \pm 0.17 \pm 0.18$ [102]. Furthermore, very recently, the CMS collaboration announced the first preliminary result of $R_{J/\psi}$ using the B parking data, $R_{J/\psi}^{\rm CMS2023} = 0.17^{+0.18}_{-0.17{\rm stat}}{}^{+0.21}_{-0.22{\rm syst}}{}^{+0.19}_{-0.18{\rm theory}}$ with the muonic τ tagging [103] and $R_{J/\psi}^{\rm CMS2024} = 1.04^{+0.50}_{-0.44}$ with the hadronic τ tagging [104]. By naively averaging them, we obtain

$$R_{J/\psi} = 0.61 \pm 0.18, \tag{1.9}$$

which is consistent with the SM prediction [43] at 1.9σ level, see Table II. Although these results still have large experimental uncertainties, it would be useful in the future to test some NP scenarios for the sake of the $R_{D^{(*)}}$ anomalies. We update the numerical formula for $R_{J/\psi}$ in the presence of general NP contributions and put a prediction from our fit study.

(2) The Υ leptonic decays, $\Upsilon \to l^+l^-$, are potentially connected to $R_{D^{(*)}}$ once one specifies NP interactions to the bottom quark and leptons. Although the SM contribution comes from a photon exchange, it is suppressed by the Υ mass squared. The sensitivity to NP is, therefore, not completely negligible, and the LFU of $R_{\Upsilon(nS)} \equiv \mathcal{B}(\Upsilon(nS) \to \tau^+\tau^-)/\mathcal{B}(\Upsilon(nS) \to \ell^+\ell^-)$ can be an important cross check of the $R_{D^{(*)}}$ anomalies. Furthermore, the *BABAR* collaboration has reported a result that slightly violates the LFU: $R_{\Upsilon(3S)} = 0.966 \pm 0.008 \pm 0.014$ [105]. We investigate the theoretical correlations in several NP models.

This paper is organized as follows. In Sec. II, we put the numerical formulas for the relevant observables in terms of the effective Hamiltonian. We also summarize the case for single-operator analysis. In Sec. III, based on the generic study with renormalization-group running effects, we obtain relations among R_D, R_{D^*}, and $F_L^{D^*}$ in the LQ models and discuss their potential to explain the present data. Relations to the τ polarizations are also discussed. In Sec. IV, we also investigate the LFU violation in the Υ decays and show its correlation with $b \to c\tau\bar{\nu}$ observables. Finally, we conclude in Sec. V and correlations in the precision measurements for each NP scenario are summarized in Table VI.

II. GENERAL FORMULAS FOR THE OBSERVABLES

At first, we describe general NP contributions to $b \to c\tau\bar{\nu}$ in terms of the effective Hamiltonian. The operators relevant to the processes of interest are described as[2]

$$\begin{aligned}\mathcal{H}_{\rm eff} = 2\sqrt{2}G_F V_{cb}[&(1 + C_{V_L})O_{V_L} + C_{V_R}O_{V_R} \\ &+ C_{S_L}O_{S_L} + C_{S_R}O_{S_R} + C_T O_T],\end{aligned} \tag{2.1}$$

with

$$\begin{aligned}&O_{V_L} = (\bar{c}\gamma^\mu P_L b)(\bar{\tau}\gamma_\mu P_L \nu_\tau), \quad O_{V_R} = (\bar{c}\gamma^\mu P_R b)(\bar{\tau}\gamma_\mu P_L \nu_\tau), \\ &O_{S_L} = (\bar{c}P_L b)(\bar{\tau}P_L \nu_\tau), \quad O_{S_R} = (\bar{c}P_R b)(\bar{\tau}P_L \nu_\tau), \\ &O_T = (\bar{c}\sigma^{\mu\nu}P_L b)(\bar{\tau}\sigma_{\mu\nu}P_L \nu_\tau),\end{aligned} \tag{2.2}$$

where $P_L = (1 - \gamma_5)/2$ and $P_R = (1 + \gamma_5)/2$. The NP contribution is encoded in the Wilson coefficients (WCs) of C_X, normalized by the SM factor of $2\sqrt{2}G_F V_{cb}$. The SM corresponds to $C_X = 0$ for $X = V_{L,R}$, $S_{L,R}$, and T in this description. We assume that the light neutrino is always

[2]The different naming schemes of the operators are often used [106–108]. Our $C_{V_L}, C_{V_R}, C_{S_L}$, and C_{S_R} correspond to $C_{V_1}, C_{V_2}, C_{S_2}$, and C_{S_1}, respectively.

left-handed and NP contributions are relevant to only the third-generation leptons (τ, ν_τ).[3]

Note that the leading $SU(2)_L \times U(1)_Y$ invariant operator, to generate the LFU violated type of the O_{V_R} form, is given in dimension eight as $(\bar{c}_R \gamma^\mu b_R)(\bar{L}^3 \gamma_\mu \tau^A L^3)(\tilde{H}\tau^A H)$. This implies that C_{V_R} in a NP model necessarily has an additional suppression compared with the other operators generated from dimension-six operators. See Ref. [117] for a NP model that can generate the C_{V_R} contributions to $R_{D^{(*)}}$.

In the following parts, the observables for $\bar{B} \to D^{(*)}\tau\bar{\nu}$, $B_c \to \tau\bar{\nu}$, and $B_c \to J/\psi\tau\bar{\nu}$ are evaluated with Eq. (2.1) at the scale $\mu = \mu_b = 4.18$ GeV. The process $\Upsilon(nS) \to l^+l^-$ will be described in detail in Sec. IV.

A. $\bar{B} \to D^{(*)}\tau\bar{\nu}$

In this work, we follow analytic forms of the differential decay rates for $\bar{B} \to D^{(*)}\tau\bar{\nu}$ obtained in Refs. [106,118]. Regarding the form factors, we employ the general HQET-based description [31] in which the heavy quark expansions [34,119] are taken up to NLO for $\epsilon_a = \alpha_s/\pi$, $\epsilon_b = \bar{\Lambda}/(2m_b)$ and NNLO for $\epsilon_c = \bar{\Lambda}/(2m_c)$ by recalling the fact $\epsilon_a \sim \epsilon_b \sim \epsilon_c^2$. Thanks to HQET property, the form factors for the different Lorenz structures of the NP operators are connected to that for the SM current, which enables us to evaluate the NP contributions to the observables.

Two parametrization models have been considered with respect to the $z = (\sqrt{w+1} - \sqrt{2})/(\sqrt{w+1} + \sqrt{2})$ expansions for the form factors in this description, with which the most general fit analyses of the form-factor parameters and $|V_{cb}|$ have been performed in Ref. [30]. For the present work, we take the $(2/1/0)$ model with a minor update and apply the updated fit result based on Ref. [30].

We have evaluated the ratio observables, $R_{D^{(*)}}$, $P_\tau^{D^{(*)}}$, and $F_L^{D^*}$, for the case of the effective Hamiltonian of Eq. (2.1) at the scale $\mu = \mu_b$. In the end, we find the following updated numerical formulas,

$$\begin{aligned}\frac{R_D}{R_D^{\rm SM}} &= |1 + C_{V_L} + C_{V_R}|^2 + 1.01|C_{S_L} + C_{S_R}|^2 + 0.84|C_T|^2 \\ &\quad + 1.49{\rm Re}\left[(1 + C_{V_L} + C_{V_R})(C_{S_L}^* + C_{S_R}^*)\right] \\ &\quad + 1.08{\rm Re}\left[(1 + C_{V_L} + C_{V_R})C_T^*\right], \end{aligned} \tag{2.3}$$

$$\begin{aligned}\frac{R_{D^*}}{R_{D^*}^{\rm SM}} &= |1 + C_{V_L}|^2 + |C_{V_R}|^2 + 0.04|C_{S_L} - C_{S_R}|^2 + 16.0|C_T|^2 \\ &\quad - 1.83{\rm Re}[(1 + C_{V_L})C_{V_R}^*] - 0.11{\rm Re}[(1 + C_{V_L} - C_{V_R})(C_{S_L}^* - C_{S_R}^*)] \\ &\quad - 5.17{\rm Re}[(1 + C_{V_L})C_T^*] + 6.60{\rm Re}[C_{V_R}C_T^*], \end{aligned} \tag{2.4}$$

$$\begin{aligned}\frac{P_\tau^D}{P_{\tau,{\rm SM}}^D} &= \left(\frac{R_D}{R_D^{\rm SM}}\right)^{-1} \times (|1 + C_{V_L} + C_{V_R}|^2 + 3.04|C_{S_L} + C_{S_R}|^2 + 0.17|C_T|^2 \\ &\quad + 4.50{\rm Re}[(1 + C_{V_L} + C_{V_R})(C_{S_L}^* + C_{S_R}^*)] - 1.09{\rm Re}[(1 + C_{V_L} + C_{V_R})C_T^*]), \end{aligned} \tag{2.5}$$

$$\begin{aligned}\frac{P_\tau^{D^*}}{P_{\tau,{\rm SM}}^{D^*}} &= \left(\frac{R_{D^*}}{R_{D^*}^{\rm SM}}\right)^{-1} \times (|1 + C_{V_L}|^2 + |C_{V_R}|^2 - 0.07|C_{S_R} - C_{S_L}|^2 - 1.85|C_T|^2 \\ &\quad - 1.79{\rm Re}[(1 + C_{V_L})C_{V_R}^*] + 0.23{\rm Re}[(1 + C_{V_L} - C_{V_R})(C_{S_L}^* - C_{S_R}^*)] \\ &\quad - 3.47{\rm Re}[(1 + C_{V_L})C_T^*] + 4.41{\rm Re}[C_{V_R}C_T^*]), \end{aligned} \tag{2.6}$$

$$\begin{aligned}\frac{F_L^{D^*}}{F_{L,{\rm SM}}^{D^*}} &= \left(\frac{R_{D^*}}{R_{D^*}^{\rm SM}}\right)^{-1} \times (|1 + C_{V_L} - C_{V_R}|^2 + 0.08|C_{S_L} - C_{S_R}|^2 + 6.90|C_T|^2 \\ &\quad - 0.25{\rm Re}[(1 + C_{V_L} - C_{V_R})(C_{S_L}^* - C_{S_R}^*)] - 4.30{\rm Re}[(1 + C_{V_L} - C_{V_R})C_T^*]), \end{aligned} \tag{2.7}$$

which can be compared with those in the literature [59,60,110,114,120]. The SM predictions are obtained as[4]

[3]See Refs. [109–115] for models with the right-handed neutrino ν_R. It is noted that the W' is necessarily accompanied by Z' and thus the recent di-τ resonance search [100,101] excludes the W'_R explanation [116].

[4]We updated the fit analysis with the modification of the formula for unitarity bound [119], pointed out by Ref. [121]. It only affects the last digits of the SM predictions, though.

$$\begin{aligned} R_D^{\rm SM} &= 0.290 \pm 0.003, \\ R_{D^*}^{\rm SM} &= 0.248 \pm 0.001, \\ P_{\tau,{\rm SM}}^{D} &= 0.331 \pm 0.004, \\ P_{\tau,{\rm SM}}^{D^*} &= -0.497 \pm 0.007, \\ F_{L,{\rm SM}}^{D^*} &= 0.464 \pm 0.003. \end{aligned} \tag{2.8}$$

Furthermore, we have checked uncertainties of the above numerical coefficients in the formulae, based on the fit result from Ref. [30]. The tensor (scalar) terms involve $\sim 4\%(10\%)$ uncertainties for the D (D^*) mode, while the others contain less than 1% errors. At present, they are not significant and thus neglected in our following study.

B. $B_c \to \tau\bar{\nu}$

The significant constraint on the scalar operators $O_{S_{L,R}}$ comes from the B_c lifetime measurements (τ_{B_c}) [82,122–125]: the branching ratio of $B_c^- \to \tau\bar{\nu}$, which has not yet been observed, is significantly amplified by the NP scalar interactions, and the branching ratio is constrained from measured τ_{B_c} [126]. We obtain an upper bound on the WCs as

$$\begin{aligned} &|1 + C_{V_L} - C_{V_R} - 4.35(C_{S_L} - C_{S_R})|^2 \\ &\quad = \frac{\mathcal{B}(B_c \to \tau\bar{\nu})}{\mathcal{B}(B_c \to \tau\bar{\nu})_{\rm SM}} < 27.1\left(\frac{\mathcal{B}(B_c \to \tau\bar{\nu})_{\rm UB}}{0.6}\right), \end{aligned} \tag{2.9}$$

with $\mathcal{B}(B_c \to \tau\bar{\nu})_{\rm SM} \simeq 0.022$. Throughout this paper, $|V_{cb}| = (41.0 \pm 1.4) \times 10^{-3}$ is used unless otherwise mentioned [126]. The b and c quark mass inputs, which are relevant for scalar contributions, are taken as $m_b(\mu_b) = (4.18 \pm 0.03)$ GeV and $m_c(\mu_b) = (0.92 \pm 0.02)$ GeV. Reference [123] evaluated that the upper bound (UB) on the branching ratio from τ_{B_c} is $\mathcal{B}(B_c \to \tau\bar{\nu})_{\rm UB} = 0.3$. However, it is pointed out by Ref. [60] and later confirmed by Ref. [125] that there is a sizeable charm-mass dependence on the B_c decay rate because the dominant contribution comes from the charm-quark decay into strange within the B_c meson. A conservative bound is set by Ref. [60] as $\mathcal{B}(B_c \to \tau\bar{\nu})_{\rm UB} = 0.6$.

One should note that more aggressive bound $\mathcal{B}(B_c \to \tau\bar{\nu})_{\rm UB} = 0.1$ has been obtained in Ref. [127] by using LEP data. However, it is pointed out that p_T dependence of the fragmentation function, $b \to B_c$, has been entirely overlooked, and thus the bound must be overestimated by several factors [60,61,128]. Although the CEPC and FCC-ee experiments are in the planning stages, the future Tera-Z machines can directly measure $\mathcal{B}(B_c \to \tau\bar{\nu})$ at O(1%) level [129–131].

Thanks to the conservative bound, the left-handed scalar operator, C_{S_L} comes back to the game. For instance, a general two-Higgs doublet model is a viable candidate, and readers are referred to Refs. [132,133].

C. $B_c \to J/\psi\tau\bar{\nu}$

We follow the form factor description from the recent lattice result of Ref. [134] for $B_c \to J/\psi\tau\bar{\nu}$. We also take $m_b(\mu_b)$ and $m_c(\mu_b)$ for the scalar and tensor sectors as aforementioned. The formula for $R_{J/\psi}$ is given as

$$\begin{aligned} \frac{R_{J/\psi}}{R_{J/\psi}^{\rm SM}} &= |1 + C_{V_L}|^2 + |C_{V_R}|^2 + 0.04|C_{S_L} - C_{S_R}|^2 + 14.7|C_T|^2 \\ &\quad - 1.82{\rm Re}[(1 + C_{V_L})C_{V_R}^*] - 0.10{\rm Re}[(1 + C_{V_L} - C_{V_R})(C_{S_L}^* - C_{S_R}^*)] \\ &\quad - 5.39{\rm Re}[(1 + C_{V_L})C_T^*] + 6.57{\rm Re}[C_{V_R}C_T^*], \end{aligned} \tag{2.10}$$

where we take $R_{J/\psi}^{\rm SM} = 0.258 \pm 0.004$ [43]. The coefficients potentially have 10–20% uncertainties for $C_{S_{L,R}}$ and C_T, while a few percent for $C_{V_{L,R}}$.

It is also known that there is a good NP correlation in the general effective Hamiltonian [124,135]

$$\frac{R_{J/\psi}}{R_{J/\psi}^{\rm SM}} \simeq \frac{R_{D^*}}{R_{D^*}^{\rm SM}}. \tag{2.11}$$

This is because both channels are the scalar to vector-meson transitions. Taking the aforementioned averages of $R_{J/\psi}^{\rm exp}$ and $R_{D^*}^{\rm exp}$, we see

$$\frac{R_{J/\psi}^{\rm exp}}{R_{J/\psi}^{\rm SM}} - \frac{R_{D^*}^{\rm exp}}{R_{D^*}^{\rm SM}} = 1.2 \pm 0.7, \tag{2.12}$$

which shows 1.7σ deviations from the prediction of Eq. (2.11) for now but it is not conclusive due to large uncertainty from $R_{J/\psi}^{\rm exp}$.

D. $\Lambda_b \to \Lambda_c\tau\bar{\nu}$

A baryonic counterpart of the $b \to c\tau\bar{\nu}$ decay is $\Lambda_b \to \Lambda_c\tau\bar{\nu}$. Normalizing by the light-lepton channels, the LFU observable R_{Λ_c} is defined, $R_{\Lambda_c} \equiv \mathcal{B}(\Lambda_b \to \Lambda_c\tau\bar{\nu})/\mathcal{B}(\Lambda_b \to \Lambda_c\ell\bar{\nu})$. Similar to the $R_{D^{(*)}}$, the CKM dependence completely drops out and the form-factor uncertainties are significantly reduced in R_{Λ_c} [44,136–141].

Furthermore, since there is no subleading Isgur-Wise function at $\mathcal{O}(\bar{\Lambda}/m_{c,b})$ in the $\Lambda_b \to \Lambda_c$ transition, the theoretical uncertainty is even suppressed [142]. As one can easily imagine, $R_{D^{(*)}}$ and R_{Λ_c} have a strong theoretical correlation through the $b \to c\tau\bar{\nu}$ interaction. NP contributions with these correlations have been widely investigated including the forward-backward asymmetry of τ, the longitudinal polarizations of Λ_c and τ, and a leptonic energy distribution [60,61,143–149].

Based on the lattice QCD results for the $\Lambda_b \to \Lambda_c$ transition [138,140,146], we obtain a numerical formula of R_{Λ_c} [150]

$$\begin{aligned}\frac{R_{\Lambda_c}}{R_{\Lambda_c}^{\rm SM}} &= |1+C_{V_L}|^2 + |C_{V_R}|^2 - 0.72{\rm Re}[(1+C_{V_L})C_{V_R}^*] + 0.50{\rm Re}[(1+C_{V_L})C_{S_R}^* + C_{V_R}C_{S_L}^*] \\ &\quad + 0.33{\rm Re}[(1+C_{V_L})C_{S_L}^* + C_{V_R}C_{S_R}^*] + 0.52{\rm Re}[C_{S_L}C_{S_R}^*] + 0.32(|C_{S_L}|^2 + |C_{S_R}|^2) \\ &\quad - 3.11{\rm Re}[(1+C_{V_L})C_T^*] + 4.88{\rm Re}[C_{V_R}C_T^*] + 10.4|C_T|^2, \end{aligned} \tag{2.13}$$

where we again take the same $m_b(\mu_b)$ and $m_c(\mu_b)$ as above for the form factors of the scalar and pseudoscalar currents. The SM prediction is $R_{\Lambda_c}^{\rm SM} = 0.324 \pm 0.004$ [44,141], where the LHCb data of $d\Gamma(\Lambda_b \to \Lambda_c\mu\bar{\nu})/dq^2$ [151] is used for a fit of their HQET parameters, in addition to the lattice QCD form factor calculations.

It is known that there is a sum rule between R_{Λ_c} and $R_{D^{(*)}}$ [60,61,150]

$$\frac{R_{\Lambda_c}}{R_{\Lambda_c}^{\rm SM}} = 0.280\frac{R_D}{R_D^{\rm SM}} + 0.720\frac{R_{D^*}}{R_{D^*}^{\rm SM}} + \delta_{\Lambda_c}, \tag{2.14}$$

with

$$\begin{aligned}\delta_{\Lambda_c} &= {\rm Re}[(1+C_{V_L})(0.035C_{V_R}^* - 0.003C_{S_R}^* + 0.314C_T^*)] - {\rm Re}[C_{V_R}(0.003C_{S_L}^* + 0.175C_T^*)] \\ &\quad + 0.014(|C_{S_L}|^2 + |C_{S_R}|^2) - 1.30|C_T|^2 + 0.004{\rm Re}[C_{S_L}C_{S_R}^*]. \end{aligned} \tag{2.15}$$

As far as $|C_T| \ll 1$ holds, δ_{Λ_c} will never be relevant and this sum rule holds in any NP scenario. Ignoring the small δ_{Λ_c} term, we obtain a model-independent prediction of R_{Λ_c}

$$\begin{aligned} R_{\Lambda_c} &\simeq R_{\Lambda_c}^{\rm SM}\left(0.280\frac{R_D}{R_D^{\rm SM}} + 0.720\frac{R_{D^*}}{R_{D^*}^{\rm SM}}\right), \\ &= R_{\Lambda_c}^{\rm SM}(1.163 \pm 0.034), \\ &= 0.377 \pm 0.011_{R_{D^{(*)}}} \pm 0.005_{R_{\Lambda_c}^{\rm SM}}. \end{aligned} \tag{2.16}$$

This implies that R_{Λ_c} is not used to distinguish the NP scenarios but rather gives a consistency check among the experimental measurements. While the $\Lambda_b \to \Lambda_c\ell\bar{\nu}$ decay has been experimentally measured already with good accuracy [151–154], the $\Lambda_b \to \Lambda_c\tau\bar{\nu}$ decay had not been observed until 2022. The observed value of the LHCb collaboration is $R_{\Lambda_c}^{\rm LHCb} = 0.242 \pm 0.026_{\rm stat} \pm 0.071_{\rm syst}$ [155], which provides a 1.8σ level tension from the sum rule prediction in Eq. (2.16). Instead, normalizing with the SM prediction of $\Gamma(\Lambda_b \to \Lambda_c\mu\bar{\nu})$ improves the accuracy and slightly uplifts the central value, $R_{\Lambda_c} = |0.041/V_{cb}|^2(0.271 \pm 0.069) = 0.271 \pm 0.072$ [156]. While suppression of R_{Λ_c} compared to the sum rule prediction would not be compatible with NP scenarios for the $R_{D^{(*)}}$ anomaly, the experimental uncertainty in R_{Λ_c} is still very large to draw a clear-cut conclusion. Detailed analysis for NP scenarios for light lepton modes is given in Ref. [150].

III. FIT ANALYSIS

In this paper, we perform the following statistical analysis to probe several NP scenarios via a bottom-up approach:

(1) Three measurements of R_D, R_{D^*}, and $F_L^{D^*}$ are taken in the χ^2 fit, and then the favored regions for the NP parameter space are obtained, which are defined by $\Delta\chi^2 = \chi^2 - \chi^2_{\rm NP-best} \leq 1$.
(2) We then check whether the above solutions are consistent with the other relevant observables, such as the B_c lifetime and the LHC bounds.
(3) Furthermore, we evaluate NP predictions on P_τ^D, $P_\tau^{D^*}$, and $R_{J/\psi}$, where the above steps 1 and 2 are passed.
(4) If applicable, a combined study with $R_{\Upsilon(3S)}$ is discussed.

The χ^2 fit function in the step 1 is defined as

$$\chi^2 \equiv \sum_{i,j}(O^{\rm theory} - O^{\rm exp})_i {\rm Cov}_{ij}^{-1}(O^{\rm theory} - O^{\rm exp})_j, \tag{3.1}$$

TABLE III. The 95% CL upper bounds on the WCs at the $\mu = \mu_b$ scale from the LHC analysis of the $\tau+$ missing search [97]. The future prospects with b-tagged jet $+ \tau\nu$ final state assuming 3 ab^{-1} of accumulated data are given in the parenthesis [98]. The NP mass scale is shown as $M_{\rm LQ} = 2$ TeV, 4 TeV and $\Lambda_{\rm EFT} > 10$ TeV.

	$\lvert C_{V_L}\rvert$	$\lvert C_{V_R}\rvert$	$\lvert C_{S_L}\rvert$	$\lvert C_{S_R}\rvert$	$\lvert C_T\rvert$
EFT ($>$ 10 TeV)	0.32(0.09)	0.33(0.09)	0.55(0.14)	0.55(0.15)	0.17(0.04)
LQ (4 TeV)	0.36(0.10)	0.40(0.10)	0.74(0.17)	0.67(0.18)	0.22(0.05)
LQ (2 TeV)	0.42(0.12)	0.51(0.15)	0.80(0.22)	0.77(0.22)	0.30(0.07)

where we take into account the $R_{D^{(*)}}$ and $F_L^{D^*}$ measurements for $O^{\rm exp}$ summarized by HFLAV as shown in Sec. I. The covariance is given as $\mathrm{Cov}_{ij} = \Delta O_i^{\rm exp}\rho_{ij}\Delta O_j^{\rm exp} + \Delta O_i^{\rm theory}\delta_{ij}\Delta O_j^{\rm theory}$, where correlation ρ_{ij} is given as in Table I while $\rho_{ij} = \delta_{ij}$ among the independent measurements. For every observable, we have the theory formulas $O^{\rm theory}$ as shown in Sec. II, and hence obtain best-fit values in terms of the WCs as defined in Eq. (2.1), which are given at the μ_b scale.

Given the SM predictions as $R_D^{\rm SM} = 0.290 \pm 0.003$, $R_{D^*}^{\rm SM} = 0.248 \pm 0.001$, and $F_{L,\rm SM}^{D^*} = 0.464 \pm 0.003$ [30], we obtain $\chi^2_{\rm SM} = 23.1$ (corresponding to 4.1σ) implying a large deviation from the SM. Briefly, $\chi^2_{\rm NP-best} \le \mathcal{O}(1)$ implies an excellent fit by the NP operators, but its criterion depends on the number of the fitted WCs. In our analysis, the goodness of fit for each NP scenario (the likelihood-ratio test between the best-fit points) is expressed by the "Pull" value (defined in, e.g., Refs. [60,157]). It depends on the number of the fitted WCs. For cases of the single WC fits, the Pull is equivalent to

$$\mathrm{Pull}(\text{single WC}) = \sqrt{\chi^2_{\rm SM} - \chi^2_{\rm NP\text{-}best}}(\sigma). \qquad (3.2)$$

Therefore, Pull $\gtrsim 4$ represents an excellent NP fit, where R_D and R_{D^*} anomalies mostly can be explained at 1σ levels. Thus, we can quantitatively compare the NP scenarios by using the Pull values.

Regarding the LHC bound to be compared with the above fit result, we refer to the result from Ref. [97], in which the $\tau +$ missing searches have been analyzed. Their result is shown in Table III, where we give the 95% CL upper limit at the μ_b scale.[5] It should be emphasized that the LHC bound on the WC has a non-negligible mediator mass dependence, see Ref. [97] for details. This feature is indeed crucial for some NP scenarios, as will be seen later. Furthermore, it is pointed out that the charge asymmetry of the τ lepton will improve the bound on C_X.

[5]Note that Table 2 of Ref. [97] shows the LHC bound at $\mu = \Lambda_{\rm LHC}$.

A. EFT: Single operator scenario

We begin with the single NP operator scenarios based on the effective field theory (EFT) of Eq. (2.1). Assuming the WC to be real, we immediately obtain the fit results with the Pull values and predictions of $P_\tau^D, P_\tau^{D^*}$, and $R_{J/\psi}$ as shown in Table IV. The allowed regions from the B_c lifetime and current LHC bounds are listed as well.

For all the NP scenarios, we can see much improvement in the fit compared with the SM. A significant change from the previous conclusion (before the new LHCb results [6,15–17] came up [61,146,158]) is that the C_{S_R} scenario becomes consistent with the data within 95% CL, i.e., $\chi^2_{\rm best} < 8.0$ (for three observed data). Unfortunately, it is known that the usual type-II two-Higgs doublet model cannot achieve this solution because the sign of C_{S_R} must be negative: $C_{S_R} = -m_b m_\tau \tan^2\beta/m^2_{H^\pm} < 0$. It is noted that even in the generic two-Higgs doublet model, sizable C_{S_R} contribution is difficult due to constraints from ΔM_s and the LHC search [92,159]. Instead, the real C_{S_L} scenario is not likely to explain the present data within 2σ level. This is mainly because the coefficients of interference terms between the real C_{S_L} and the SM contribution in Eqs. (2.3) and (2.4) have opposite signs, which prevent the simultaneous explanation of $R_{D^{(*)}}$ anomalies. The situation is the same as the previous one before the new LHCb and Belle II data. The C_{V_L} scenario well explains the present data, while C_{V_R} gives a lower Pull. The C_T solution gives unique predictions on the other observables, which may be able to identify the NP scenario, and it predicts a negative shift of $F_L^{D^*}$ with a tension from the present measurement [59,70].

Once we allow complex values of WCs, the complex C_{V_R}, C_{S_L}, and C_T scenarios improve the fits such as

$$C_{V_R} \simeq +0.01 \pm i0.41 \qquad \mathrm{Pull} = 4.4, \qquad (3.3)$$

$$C_{S_L} \simeq -0.79 \pm i0.86 \qquad \mathrm{Pull} = 4.3, \qquad (3.4)$$

$$C_T \simeq +0.02 \pm i0.13 \qquad \mathrm{Pull} = 3.8, \qquad (3.5)$$

while the complex C_{V_L} and C_{S_R} scenarios give the same Pulls compared with those with the real WC scenarios. The complex C_T scenario has a similar Pull with the real C_T case due to the penalty of adding one more parameter. We

TABLE IV. The fit results of the single NP operator scenarios assuming real WCs. The WCs are given at the μ_b scale. The allowed ranges of WC from the B_c lifetime and the current LHC bounds are also shown ("very loose" represents very weak bounds). Fitted WCs and predictions of P_τ^D, $P_\tau^{D^*}$, and $R_{J/\psi}$ are in the range of $\Delta\chi^2 = \chi^2 - \chi^2_{\rm best} \leq 1$.

			Allowed region of C_X		Predictions ($\Delta\chi^2 \leq 1$)		
	Pull [$\chi^2_{\rm best}$]	Fitted C_X	$B_c \to \tau\bar{\nu}$	LHC	P_τ^D	$-P_\tau^{D^*}$	$R_{J/\psi}$
SM	$-[23.1]$	⋯	⋯	⋯	0.331 ± 0.004	0.497 ± 0.007	0.258 ± 0.004
C_{V_L}	4.8[0.3]	$+0.079(16)$	Very loose	$[-0.32, 0.32]$	[0.331, 0.331]	[0.497, 0.497]	[0.291, 0.309]
C_{V_R}	2.6[16.3]	$-0.070(26)$	Very loose	$[-0.33, 0.33]$	[0.331, 0.331]	[0.495, 0.496]	[0.280, 0.307]
C_{S_L}	3.1[13.6]	$+0.165(48)$	$[-0.94, 1.4]$	$[-0.55, 0.55]$	[0.435, 0.508]	[0.516, 0.531]	[0.254, 0.256]
C_{S_R}	3.9[8.0]	$+0.182(42)$	$[-1.4, 0.94]$	$[-0.55, 0.55]$	[0.454, 0.516]	[0.458, 0.473]	[0.261, 0.263]
C_T	4.1[6.4]	$-0.033(7)$	⋯	$[-0.17, 0.17]$	[0.350, 0.361]	[0.457, 0.473]	[0.290, 0.311]

note that previously the C_T solution had been disfavored by the $F_L^{D^*}$ measurement [59]. However, the recent combined data revives the complex C_T solution: The fitted WC of C_T in Eq. (3.5) predicts $F_L^{D^*} \simeq 0.41$ which is consistent with the measured value within 2σ level, and hence the near future data will be crucial to test the scenario. The complex C_{V_R} result at the above best-fit point is, however, not consistent with the LHC bound for the case of EFT, $|C_{V_R}| < 0.33$. Nevertheless, it could be relaxed in some LQ models with the mass of the LQ particle to be $M_{\rm LQ} \gtrsim 2$ TeV as seen in Table III.

As for the complex C_{S_L} scenario, since the imaginary part does not interfere with the SM contribution, the situation is different from the real C_{S_L} scenario, and the $R_{D^{(*)}}$ anomalies can be explained. It, however, looks like the best-fit point in Eq. (3.4) is disfavored by the LHC and B_c lifetime constraints. Yet, it is noted that the LHC bound is not always proper and depends on the NP model. In the case of the charged-Higgs model, for instance, the bound on the s-channel mediator $H^\pm$ significantly depends on the resonant mass. Experimentally, it is not easy to probe the low mass $\tau\nu$ resonance due to the huge SM W background. Reference [132] points out that the range of $m_t \leq m_{H^\pm} \leq 400$ GeV is still viable for the 1σ explanation, although LHC run 2 data is already enough to probe this range if the $\tau\nu + b$ and $t + \tau\tau$ signatures are searched [133,160]. Thus, we leave the LHC bound for the complex C_{S_L} scenario below. Once the B_c bound of Eq. (2.9) with $\mathcal{B}(B_c \to \tau\bar{\nu})_{\rm UB} = 0.6$ is imposed, we find

$$C_{S_L} \simeq -0.57 \pm i0.86 \qquad \text{Pull} = 4.3, \tag{3.6}$$

for the best Pull within the constraint. The same pull is obtained as in Eq. (3.4) within the digit that we consider.

It has been pointed out that q^2 distributions in $d\Gamma(\bar{B} \to D^{(*)}\tau\bar{\nu})/dq^2$ and $dR_{D^{(*)}}/dq^2$ are sensitive to the scalar contribution [82,118]. Furthermore, it is pointed out that a LFU ratio similar to $R_{D^{(*)}}$ with the q^2 integration starting from m_τ^2 commonly in both τ and ℓ modes, so-called $\tilde{R}_{D^{(*)}}$ will be significant [78,161]. We do not consider the constraint since the experimental data is not conclusive. In any case, the Belle II data will be important [108].

In Fig. 2, we show predictions on the plane of $P_\tau^D - P_\tau^{D^*}$ evaluated from our fit analysis with each complex WC scenario. The allowed regions satisfying $\Delta\chi^2 \leq 1$ (4) are shown in dark (light) orange, brown, and blue for the complex C_{S_L}, C_{S_R}, and C_T scenarios, respectively, where the B_c lifetime and LHC bounds based on the EFT framework are also taken into account. The $C_{V_{L,R}}$ scenarios do not deviate P_τ^D and $P_\tau^{D^*}$ from the SM predictions as shown with the black dot in the figure. Also note that each shaded region is based on different Pull values, implying different significance, in Fig. 2. We can see that the correlation in τ polarization observables provides unique predictions that can identify the NP scenarios. On the other hand, $R_{J/\psi}$ is less helpful to distinguish the different operators.

B. Leptoquark scenarios

Finally, we study several LQ scenarios. It is well known that three categories of LQs can address the $R_{D^{(*)}}$ anomalies [106], which are referred to as a $SU(2)_L$-singlet vector U_1^μ, a $SU(2)_L$-singlet scalar S_1, and a $SU(2)_L$-doublet scalar R_2. The relevant LQ interactions are given in the Appendix.

A key feature with respect to the fit is that these LQ scenarios involve three independent couplings relevant for $b \to c\tau\nu$, which are encoded in terms of the two independent (and complex in general) WCs as

$$\mathrm{U}_1^\mu : C_{V_L}, C_{S_R}, \tag{3.7}$$

$$\mathrm{S}_1 : C_{V_L}, C_{S_L} = -4C_T, \tag{3.8}$$

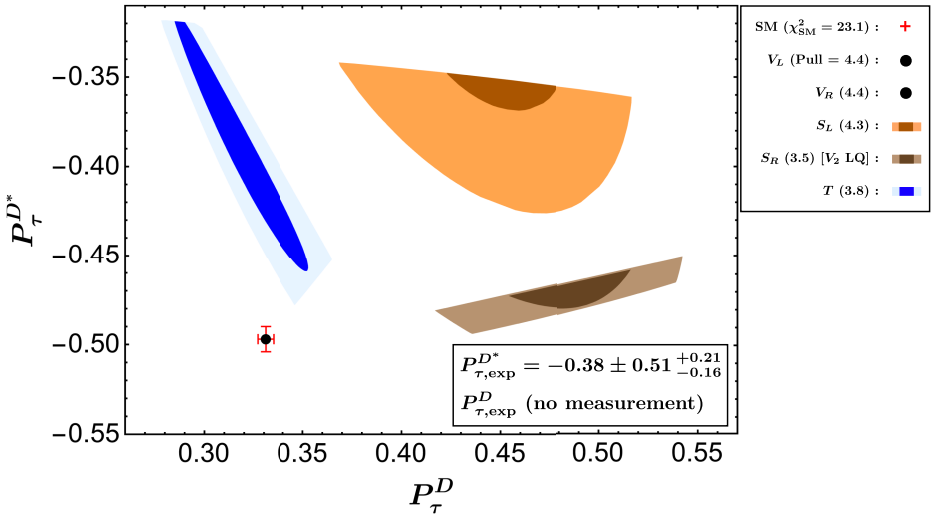

FIG. 2. Predictions of P^D_τ and $P^{D^*}_\tau$ in the complex NP operator scenarios. The allowed regions satisfying $\Delta\chi^2 \leq 1$ (4) are shown in dark (light) orange, brown, and blue for the C_{S_L}, C_{S_R}, and C_T scenarios, respectively, whereas the black dot is the case for the $C_{V_{L,R}}$ scenarios. The B_c lifetime and LHC bounds are also taken into account. The LHC bound is not taken as discussed in the main text.

$$\mathrm{R}_2 : C_{V_R}, C_{S_L} = 4C_T, \tag{3.9}$$

at the LQ scale $\Lambda_{\rm LQ} = M_{\rm LQ}$.

In addition, the $SU(2)_L$-doublet vector LQ V_2 forms C_{S_R} [106], equivalent to the single C_{S_R} scenario, and hence this LQ has now the viable solution as seen in Sec. III A:

$$\mathrm{V}_2^\mu : C_{S_R}, \tag{3.10}$$

at the LQ scale. The relations between the WC and V_2 LQ couplings are also described in the Appendix. In Refs. [162,163], phenomenology of the flavor and collider physics of the V_2 LQ scenario is investigated. It is found that the coupling product which explains $R_{D^{(*)}}$ also modifies $B_u \to \tau\bar{\nu}$, $B_s \to \tau\bar{\tau}$, and $B \to K^{(*)}\tau\bar{\tau}$ in flavor physics, and the $\tau\bar{\tau}$ final state search at LHC will be the key probe of the model.

The C_{V_L} phase in $|1 + C_{V_L}|^2$ can be absorbed [59] in the flavor process. Thus, the absorption of the C_{V_L} phase is irrelevant for the fit within the flavor observables and we take C_{V_L} in U_1 and S_1 LQs as real without loss of generality.[6] As for C_{V_R} in the R_2 LQ, we assume it as pure imaginary from the fact of Eq. (3.3). Therefore, the three LQ scenarios of our interest have three degrees of freedom for the fit and the relevant observables, and then it is expected that fit results and their predictions could be different from the previous studies.

These years, UV completions of the LQ scenarios have been studied in the literature; Refs. [164–179] for U_1, Refs. [180–182] for S_1, Refs. [183,184] for R_2, and see also Refs. [185,186]. In the next subsection, we consider the case if the U_1 LQ is induced by a UV completed theory that gives a specific relation to the LQ couplings, and see how it changes the fit result. Recent reevaluations on mass differences of the neutral B mesons ΔM_d, ΔM_s, (improved by HQET sum rule and lattice calculations [187]), would constrain a UV-completed TeV-scale LQ model [166,167,179,181,188,189]. In particular, the ratio $\Delta M_d/\Delta M_s$ provides a striking constraint on the coupling texture of the LQ interactions. Here, we comment that a typical UV completion requires a vectorlike lepton (VLL) and it induces additional LQ-VLL box diagrams that also contribute to $\Delta M_{d,s}$ destructively. This implies that the constraint from $\Delta M_{d,s}$ depends on the vectorlike fermion mass spectrum, and hence we do not consider $\Delta M_{d,s}$ further in our analysis. (Currently, the mass of the third-generation VLL is constrained to be $\gtrsim$0.5 TeV by collider searches [167,190,191], which is a milder bound than conventional searches in τh and τZ decay channels ($\gtrsim$1 TeV) [191,192]. This is because in such a model the VLL mainly undergoes LQ-mediated three-body decays.)

The LQ mass has been directly constrained as $M_{\rm LQ} \gtrsim 1.5$ TeV from the LQ pair production searches [193–195]. Hence we take $M_{\rm LQ} = 2$ TeV for our benchmark scale. We recap that the WCs are bounded from the $\tau +$ missing search and, as shown in Table III, the LQ scenarios receive milder constraints than the EFT operators as long as $M_{\rm LQ} \leq 10$ TeV.

The WCs will be fitted at the μ_b scale in our analysis, and then they are related to the WCs defined at the $\Lambda_{\rm LQ} = M_{\rm LQ}$ scale. The renormalization-group equations (RGEs) (the

[6]Now the real C_{V_L} fit to the $R_{D^{(*)}}$ anomalies gives the minimum $|C_{V_L}|$, and thus is less constrained from the LHC data.

first matrix below) [196–198] and the LQ-charge independent QCD one-loop matching (the second one) [199] gives the following relation

$$\begin{pmatrix} C_{V_L}(\mu_b) \\ C_{V_R}(\mu_b) \\ C_{S_L}(\mu_b) \\ C_{S_R}(\mu_b) \\ C_T(\mu_b) \end{pmatrix} \simeq \begin{pmatrix} 1 & 0 & 0 & 0 & 0 \\ 0 & 1 & 0 & 0 & 0 \\ 0 & 0 & 1.82 & 0 & -0.35 \\ 0 & 0 & 0 & 1.82 & 0 \\ 0 & 0 & -0.004 & 0 & 0.83 \end{pmatrix} \begin{pmatrix} 1.12 & 0 & 0 & 0 & 0 \\ 0 & 1.07 & 0 & 0 & 0 \\ 0 & 0 & 1.05 & 0 & 0 \\ 0 & 0 & 0 & 1.10 & 0 \\ 0 & 0 & 0 & 0 & 1.07 \end{pmatrix} \begin{pmatrix} C_{V_L}(\Lambda_{\mathrm{LQ}}) \\ C_{V_R}(\Lambda_{\mathrm{LQ}}) \\ C_{S_L}(\Lambda_{\mathrm{LQ}}) \\ C_{S_R}(\Lambda_{\mathrm{LQ}}) \\ C_T(\Lambda_{\mathrm{LQ}}) \end{pmatrix}$$
$$\simeq \begin{pmatrix} 1.12 & 0 & 0 & 0 & 0 \\ 0 & 1.07 & 0 & 0 & 0 \\ 0 & 0 & 1.91 & 0 & -0.38 \\ 0 & 0 & 0 & 2.00 & 0 \\ 0 & 0 & 0. & 0 & 0.89 \end{pmatrix} \begin{pmatrix} C_{V_L}(\Lambda_{\mathrm{LQ}}) \\ C_{V_R}(\Lambda_{\mathrm{LQ}}) \\ C_{S_L}(\Lambda_{\mathrm{LQ}}) \\ C_{S_R}(\Lambda_{\mathrm{LQ}}) \\ C_T(\Lambda_{\mathrm{LQ}}) \end{pmatrix}, \tag{3.11}$$

with $\Lambda_{\mathrm{LQ}} = 2$ TeV. Using these numbers, we obtain $C_{S_L}(\mu_b) = -8.9 C_T(\mu_b)$ and $C_{S_L}(\mu_b) = 8.4 C_T(\mu_b)$ for S_1 and R_2 LQs, respectively.

With these ingredients, the LQ scenarios in terms of $C_X(\mu_b)$ up to three degrees of freedom are investigated, where the full variable case is referred to as the general LQ. The results of the best-fit points for the general LQ scenarios that are also allowed from the B_c and LHC bounds are then summarized as

$$\mathrm{U_1LQ}\colon\ C_{V_L} = 0.07, \qquad C_{S_R} = 0.02, \qquad \mathrm{Pull} = 4.1, \tag{3.12}$$

$$\mathrm{S_1LQ}\colon\ C_{V_L} = 0.07, \qquad C_{S_L} = -8.9 C_T = \pm i 0.15, \qquad \mathrm{Pull} = 4.1, \tag{3.13}$$

$$\mathrm{R_2LQ}\colon\ C_{V_R} = \pm i 0.50, \qquad C_{S_L} = 8.4 C_T = 0.03 \mp i 0.18, \qquad \mathrm{Pull} = 4.1. \tag{3.14}$$

We observe that these three general LQ scenarios have the same Pull, which means they are equivalently favored by the current data. We see that at the best-fit points the U_1, S_1, and R_2 LQ scenarios prefer purely real, purely imaginary, and complex scalar NP contributions, respectively.

Regarding the general S_1 LQ scenario, we comment that a part of the allowed parameter region is ruled out by the $B \to K^* \nu \bar{\nu}$ measurement and ΔM_s (via LQ-ν_τ box) [98,189,200], although these constraints can be avoided by tuning the LQ couplings ($y_L^{b\tau} \gg y_L^{s\tau}$ defined in Eq. (A4) which leads to $C_{V_L} \simeq 0$).

Furthermore, we also investigate two restricted LQ scenarios; S_1 LQ with $C_{V_L} = 0$ and R_2 LQ with $C_{V_R} = 0$. The former scenario naturally avoids the severe constraint from ΔM_s without introducing the VLLs [98]. The latter scenario is also natural in light of the naive dimensional analysis, where the C_{V_R} contribution corresponds to the dimension-eight operator in the EFT as mentioned in Sec. II. The fit results for the S_1 LQ with $C_{V_L} = 0$ and the R_2 LQ with $C_{V_R} = 0$ are obtained as

$$\mathrm{S_1LQ}(C_{V_L} = 0)\colon\ C_{S_L} = -8.9 C_T = 0.18, \qquad \mathrm{Pull} = 4.1, \tag{3.15}$$

$$\mathrm{R_2LQ}(C_{V_R} = 0)\colon\ C_{S_L} = 8.4 C_T = -0.09 \pm i 0.56, \quad \mathrm{Pull} = 4.4, \tag{3.16}$$

where the improvements of Pull only come from the benefit of reducing the degrees of freedom.

In turn, we evaluate the LHC bounds on the two independent variables, such as (C_{V_L}, C_{S_R}) for the U_1 LQ scenario, by the following interpretations:

$$\mathrm{U_1LQ}\colon\ \frac{|C_{V_L}(\mu_b)|^2}{(0.42)^2} + \frac{|C_{S_R}(\mu_b)|^2}{(0.77)^2} < 1, \tag{3.17}$$

$$\mathrm{S_1LQ}\colon\ \frac{|C_{V_L}(\mu_b)|^2}{(0.42)^2} + \frac{|C_{S_L}(\mu_b)|^2}{(0.80)^2} < 1, \tag{3.18}$$

$$\mathrm{R_2LQ}\colon\ \frac{|C_{V_R}(\mu_b)|^2}{(0.51)^2} + \frac{|C_{S_L}(\mu_b)|^2}{(0.80)^2} < 1, \tag{3.19}$$

TABLE V. The fit results of the U_1, S_1, and R_2 LQ scenarios for $M_{LQ} = 2$ TeV. The WCs are given at the μ_b scale, whose allowed ranges are cut by the B_c lifetime and the LHC bounds. The structure is the same as in Table IV.

			Allowed region of C_X		Predictions ($\Delta\chi^2 \leq 1$)		
	Pull $[\chi^2_{\rm best}]$	Fitted C_X	$B_c \to \tau\bar{\nu}$	LHC	P_τ^D	$-P_\tau^{D^*}$	$R_{J/\psi}$
SM	$-[23.1]$	⋯	⋯	⋯	0.331 ± 0.004	0.497 ± 0.007	0.258 ± 0.004
U_1 LQ	4.1[0.2]	C_{V_L}: $[+0.048, +0.104]$ $\mathrm{Re}C_{S_R}$: $[-0.058, +0.090]$ $\mathrm{Im}C_{S_R}$: $[-0.390, +0.390]$	Eq. (2.9)	Eq. (3.17)	[0.272, 0.413]	[0.482, 0.533]	[0.285, 0.311]
S_1 LQ	4.1[0.3]	C_{V_L}: $[+0.032, +0.160]$ $\mathrm{Re}C_{S_L}$: $[-0.110, +0.110]$ $\mathrm{Im}C_{S_L}$: $[-0.416, +0.416]$	Eq. (2.9)	Eq. (3.18)	[0.086, 0.442]	[0.374, 0.502]	[0.275, 0.312]
S_1 LQ ($C_{V_L} = 0$)	4.1[3.0]	$\mathrm{Re}C_{S_L}$: $[+0.014, +0.210]$ $\mathrm{Im}C_{S_L}$: $[-0.522, +0.522]$	Eq. (2.9)	Eq. (3.19)	[0.466, 0.524]	[0.456, 0.504]	[0.271, 0.284]
R_2 LQ	4.1[0.1]	$\mathrm{Im}C_{V_R}$: $[\pm 0.000, \pm 0.504]$ $\mathrm{Re}C_{S_L}$: $[-0.036, +0.054]$ $\mathrm{Im}C_{S_L}$: $[\mp 0.000, \mp 0.310]$	Eq. (2.9)	Eq. (3.19)	[0.259, 0.478]	[0.402, 0.533]	[0.280, 0.313]
R_2 LQ ($C_{V_R} = 0$)	4.4[0.6]	$\mathrm{Re}C_{S_L}$: $[-0.148, -0.042]$ $\mathrm{Im}C_{S_L}$: $[\pm 0.503, \pm 0.619]$	Eq. (2.9)	Eq. (3.19)	[0.404, 0.479]	[0.408, 0.440]	[0.278, 0.299]

where the denominators are the current LHC bounds for the single WC scenarios with $M_{LQ} = 2$ TeV from Table III. Indeed, this is a good approximation since the bound comes from the high-p_T region that suppresses the interference term between the $V_{L,R}$ and $S_{L,R}$ operators. It can be seen that the best-fit point of Eq. (3.14) for R_2 LQ is not consistent with the LHC bound in Eq. (3.19).

In Table V, we show our fit results and predictions with respect to each LQ scenario as we did for the EFT cases. It is observed that both the general LQ scenarios and the restricted LQ scenarios can largely deviate the τ polarizations from the SM predictions. This can be understood from the fact that the complex scalar WCs have large impacts on the interference terms, as can be checked from Eqs. (2.5) and (2.6), which results in a wide range of predictions.

In Fig. 3, we show the combined the τ polarization predictions on the $P_\tau^D - P_\tau^{D^*}$ plane satisfying $\Delta\chi^2 \leq 1(4)$ and the aforementioned B_c lifetime and the LHC bounds, where the general U_1, S_1, and R_2 LQ scenarios are shown in dark (light) green, magenta, and yellow regions, respectively. The U_1 and R_2 LQ scenarios produce the correlated

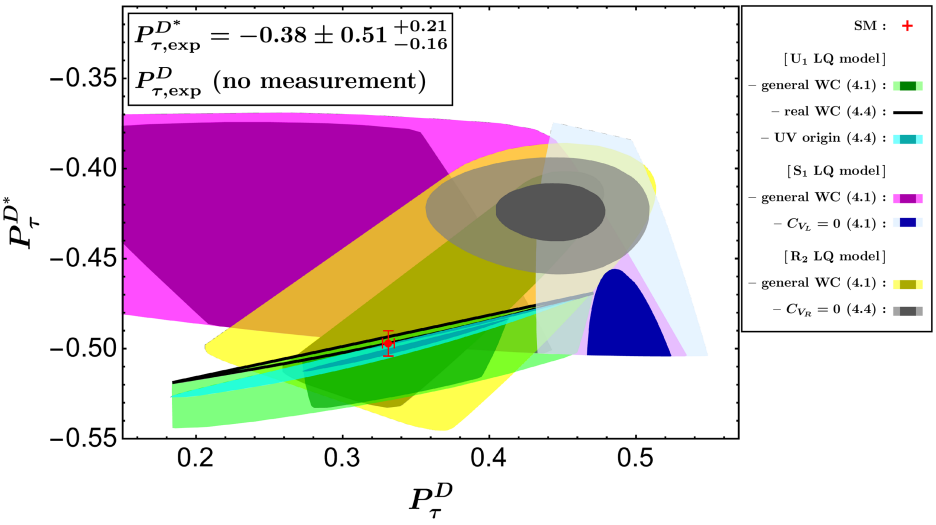

FIG. 3. Predictions of P_τ^D and $P_\tau^{D^*}$ in the LQ scenarios following the same procedure as in Fig. 2. The allowed regions are shown by dark (light) green, magenta, and yellow regions for the general U_1, S_1, and R_2 LQ scenarios, respectively. The specific scenarios; U_1 LQ with UV origin (cyan), U_1 LQ with real WCs (solid line), S_1 LQ with $C_{V_L} = 0$ (blue), and R_2 LQ with $C_{V_R} = 0$ (gray), are also shown.

regions of the P_τ^D–$P_\tau^{D^*}$ predictions and hence could be distinguished. On the other hand, the S_1 LQ scenario has a less-predictive wide region, which is hard to be identified.

Figure 3 also exhibits the predictions for several specific LQ scenarios, i.e., U_1 LQ with real C_{S_R} and C_{V_L} (solid line), S_1 LQ with $C_{V_L} = 0$ (blue region), and R_2 LQ with $C_{V_R} = 0$ (gray region). It is seen that reducing the variable in the general LQ scenario provides the distinct prediction in particular for $P_\tau^{D^*}$ and the correlation for $P_\tau^D - P_\tau^{D^*}$ becomes a useful tool to identify the LQ signature. Therefore, it is significant to restrict the LQ interactions by the τ polarization observables or by constructing a UV theory that realizes the LQ particle. The latter will be discussed in the next section for the U_1 LQ scenario, which corresponds to the cyan region in Fig. 3.

C. UV completion of U_1 leptoquark

As the U_1 LQ provides a unique solution, not only to the $b \to c\tau\nu$ anomaly but also to several flavor issues, UV completions of the U_1 LQ have been discussed enthusiastically [201–209]. A typical description is that the U_1 LQ is given as a new gauge boson, embedded in a large gauge symmetry, such that the third-generation quarks and leptons are coupled to U_1 in the interaction basis. This means that the two LQ interactions of Eq. (A1) are represented as a universal gauge coupling, $x_L^{33} = x_R^{33} \equiv g_U$ (see the Appendix). Moving to the mass basis leads to

$$C_{S_R}(\Lambda_{\rm LQ}) = -2\beta_R \times C_{V_L}(\Lambda_{\rm LQ}), \tag{3.20}$$

where $\beta_R = e^{i\phi}$ denotes the relative complex (CP-violating) phase [208], which comes from the fact that the phases in the rotation matrices (to the mass basis) for quark and lepton are not necessarily identical. The LHC bound for this scenario has been studied and the typical scale of the constraint is obtained as $\Lambda_{\rm LQ} \gtrsim 3.5$ TeV [166].

The RGE running effect changes the above relation of Eq. (3.20) at the μ_b scale of our interest. By taking $\Lambda_{\rm LQ} = 4$ TeV as a benchmark scale, we obtain

$$\begin{aligned} C_{V_L}(\mu_b) &= 1 \times 1.11 \times C_{V_L}(\Lambda_{\rm LQ}), \\ C_{S_R}(\mu_b) &= 1.90 \times 1.09 \times C_{S_R}(\Lambda_{\rm LQ}), \end{aligned} \tag{3.21}$$

where the first coefficient is the QCD two-loop RGE factor [198] and the second is the QCD one-loop matching correction [199] at the NP scale. Therefore, we have

$$C_{S_R}(\mu_b) \simeq -3.7\beta_R \times C_{V_L}(\mu_b), \tag{3.22}$$

in the case of the UV origin U_1 LQ scenario, applied to our fit analysis.

The result of the best-fit point for the UV origin U_1 LQ scenario, with the definition of $\beta_R = e^{i\phi}$, is shown as

$$(C_{V_L}, \phi) \simeq (0.075, \pm 0.466\pi) \qquad \text{Pull} = 4.4. \tag{3.23}$$

One can see that this is consistent with the B_c lifetime and LHC bounds. Predictions of the observables within $\Delta\chi^2 \le 1$, 4 are shown by the cyan region in Fig. 3. It is observed that the large complex phase is favored, which suppresses the interference while predicting nucleon electric dipole moments (d_N) within the reach of future experiments [210]. It should also be stressed that the τ polarizations are so unique that this scenario can be distinguished from the aforementioned LQ scenarios.

As briefly mentioned in the previous section, although the simplified model is severely constrained from the ΔM_s measurement (when $x_L^{s\tau} \neq 0$), it can be avoided by the existence of the VLL. There is a GIM-like mechanism including the VLL contributions, so that the bound from ΔM_s is naturally suppressed even when the VLL mass is around 1–4 TeV [166,167,174,179,181,188,211].

IV. THE LFU VIOLATION IN Υ DECAYS

The UV-completed NP models contributing to $b \to c\tau\bar{\nu}$ processes should also bring a related contribution to $b\bar{b} \to \tau^+\tau^-$ or $c\bar{c} \to \tau^+\tau^-$ interactions [45,212,213]. In this section, we show that U_1 and R_2 LQs predict a robust correlation between $b \to c\tau\bar{\nu}$ and $b\bar{b} \to \tau^+\tau^-$ via the LQ exchange.

A definition of the LFU observable in the $\Upsilon(nS)$ decays is

$$R_{\Upsilon(nS)} \equiv \frac{\mathcal{B}(\Upsilon(nS) \to \tau^+\tau^-)}{\mathcal{B}(\Upsilon(nS) \to \ell^+\ell^-)}, \tag{4.1}$$

with $n = 1, 2, 3$, where $R_{\Upsilon(nS)} \simeq 1$ holds in the SM. As for $n \ge 4$, the leptonic branching ratios are significantly suppressed since a $B\bar{B}$ decay channel is open.[7] Since the short- and long-distance QCD corrections [215] are independent of the lepton mass, they are canceled in this ratio. One can also discuss the $c\bar{c} \to l^+l^-$ LFU observable via $\psi(2S)$ decays. However, we do not consider it because the present experimental error is relatively large.

Recently, the *BABAR* collaboration has reported a precise result for the measurement of $R_{\Upsilon(3S)}$ [105]: $R_{\Upsilon(3S)}^{BABAR} = 0.966 \pm 0.008_{\rm stat} \pm 0.014_{\rm syst}$, where $\ell = \mu$. Combing a previous measurement by the CLEO collaboration [216], an average for the $\Upsilon(3S)$ decay is [212]

$$R_{\Upsilon(3S)}^{\rm exp} = 0.968 \pm 0.016. \tag{4.2}$$

This value is consistent with the SM prediction [45]

[7] A novel method for the $n = 4$ mode has been proposed in Ref. [214] by using the inclusive dileptonic channel $\Upsilon(4S) \to \ell^\pm\tau^\mp X(\bar{\nu}\nu)$, which could be probed in the Belle II experiment and is directly related to $\Gamma(b \to X\tau\nu)/\Gamma(b \to X\ell\nu)$.

$$R^{\rm SM}_{\Upsilon(3S)} = 0.9948 \pm \mathcal{O}(10^{-5}) \tag{4.3}$$

at the 1.7σ level. The SM prediction slightly deviates from 1 whose leading correction comes from the difference in the phase space factor between the τ/ℓ modes [217]. The next-to-leading contribution comes from the QED correction, which depends on the lepton mass [218]: $\delta_{\rm EM} R_{\Upsilon(nS)} = +0.0002$. The tree-level Z exchange also contributes, but its effect is $\mathcal{O}(10^{-5})$ [45]. There is no Higgs boson contribution, as one can see below. The other channels ($n = 1, 2$) still suffer from the current experimental uncertainty, and we do not utilize them in our presentation.

The effective Hamiltonian which is relevant to the bottomonium decay into $\tau^+\tau^-$ is described as

$$\begin{aligned} -\mathcal{H}^{\rm NP}_{\rm eff} = {} & C^{b\tau}_{VLL}(\bar{b}\gamma^\mu P_L b)(\bar{\tau}\gamma_\mu P_L \tau) + C^{b\tau}_{VRR}(\bar{b}\gamma^\mu P_R b)(\bar{\tau}\gamma_\mu P_R \tau) \\ & + C^{b\tau}_{VLR}(\bar{b}\gamma^\mu P_L b)(\bar{\tau}\gamma_\mu P_R \tau) + C^{b\tau}_{VRL}(\bar{b}\gamma^\mu P_R b)(\bar{\tau}\gamma_\mu P_L \tau) \\ & + [C^{b\tau}_{T}(\bar{b}\sigma^{\mu\nu} P_R b)(\bar{\tau}\sigma_{\mu\nu} P_R \tau) + C^{b\tau}_{SL}(\bar{b} P_L b)(\bar{\tau} P_L \tau) + C^{b\tau}_{SR}(\bar{b} P_R b)(\bar{\tau} P_L \tau) + \text{H.c.}] \end{aligned} \tag{4.4}$$

at the scale $\mu = m_\Upsilon$. Note that $C^{b\tau}_{VLL}, C^{b\tau}_{VRR}, C^{b\tau}_{VLR}$, and $C^{b\tau}_{VRL}$ are real coefficients, and $C^{b\tau}_{SL}$ and $C^{b\tau}_{SR}$ never contribute to the $\Upsilon(nS) \to \tau^+\tau^-$ due to $\langle 0|\bar{b}b|\Upsilon\rangle = \langle 0|\bar{b}\gamma_5 b|\Upsilon\rangle = 0$. In this convention, the partial decay width is given by [45]

$$\begin{aligned} \Gamma(\Upsilon(nS) \to \tau^+\tau^-) = {} & \frac{f_\Upsilon^2}{4\pi m_\Upsilon}\sqrt{1-4x_\tau^2}\Big[A_\Upsilon^2(1+2x_\tau^2) + B_\Upsilon^2(1-4x_\tau^2) \\ & + \frac{1}{2}C_\Upsilon^2(1-4x_\tau^2)^2 + \frac{1}{2}D_\Upsilon^2(1-4x_\tau^2) + 2A_\Upsilon C_\Upsilon x_\tau(1-4x_\tau^2)\Big], \end{aligned} \tag{4.5}$$

with

$$A_\Upsilon = \frac{4\pi\alpha}{3} + \frac{m_\Upsilon^2}{4}\left[C^{b\tau}_{VLL} + C^{b\tau}_{VRR} + C^{b\tau}_{VLR} + C^{b\tau}_{VRL} + 16x_\tau\frac{f_\Upsilon^T}{f_\Upsilon}\text{Re}(C^{b\tau}_T)\right], \tag{4.6}$$

$$B_\Upsilon = \frac{m_\Upsilon^2}{4}(C^{b\tau}_{VRR} + C^{b\tau}_{VLR} - C^{b\tau}_{VLL} - C^{b\tau}_{VRL}), \tag{4.7}$$

$$C_\Upsilon = 2m_\Upsilon^2\frac{f_\Upsilon^T}{f_\Upsilon}\text{Re}(C^{b\tau}_T), \tag{4.8}$$

$$D_\Upsilon = 2m_\Upsilon^2\frac{f_\Upsilon^T}{f_\Upsilon}\text{Im}(C^{b\tau}_T), \tag{4.9}$$

and

$$x_\tau = \frac{m_\tau}{m_\Upsilon}. \tag{4.10}$$

The f_Υ and f_Υ^T are decay constants for vector and tensor currents in Υ hadronic-matrix elements, and $f_\Upsilon = f_\Upsilon^T$ holds in the heavy quark limit, which is realized for the Υ decays [45].

Within the SM, this process is predominantly caused by the QED. Nevertheless, the photon-exchange QED contribution is suppressed by $1/m_\Upsilon^2$, and hence the NP contribution could be non-negligible [45,212,219]. In the SM, $A_\Upsilon \simeq 4\pi\alpha/3$ and $B_\Upsilon, C_\Upsilon, D_\Upsilon \simeq 0$. Setting the light lepton mass to zero and $m_\Upsilon = m_{\Upsilon(3S)} = 10.355$ GeV, we obtain the following numerical formula

$$\frac{R_{\Upsilon(3S)}}{R^{\rm SM}_{\Upsilon(3S)}} = 1 + 1.64\times10^{-3}\ \text{TeV}^2(C^{b\tau}_{VLL} + C^{b\tau}_{VRR} + C^{b\tau}_{VLR} + C^{b\tau}_{VRL}) + 6.37\times10^{-3}\ \text{TeV}^2\text{Re}(C^{b\tau}_T) + \delta_\Upsilon, \tag{4.11}$$

with

$$\begin{aligned} \delta_\Upsilon = {} & 5.22\times10^{-6}\ \text{TeV}^4(C^{b\tau}_{VLL} + C^{b\tau}_{VRR} + C^{b\tau}_{VLR} + C^{b\tau}_{VRL})\text{Re}(C^{b\tau}_T) \\ & + 6.71\times10^{-7}\ \text{TeV}^4(C^{b\tau}_{VLL} + C^{b\tau}_{VRR} + C^{b\tau}_{VLR} + C^{b\tau}_{VRL})^2 \\ & + 5.59\times10^{-7}\ \text{TeV}^4(C^{b\tau}_{VRR} + C^{b\tau}_{VLR} - C^{b\tau}_{VLL} - C^{b\tau}_{VRL})^2 \\ & + 2.51\times10^{-5}\ \text{TeV}^4[\text{Re}(C^{b\tau}_T)]^2 + 1.79\times10^{-5}\ \text{TeV}^4[\text{Im}(C^{b\tau}_T)]^2, \end{aligned} \tag{4.12}$$

where the δ_Υ term gives negligible contributions.

Let us now look into a correlation between $R_{\Upsilon(3S)}$ and $R_{D^{(*)}}$ by using the specific examples of the U_1 and R_2 LQs. First, we exhibit the U_1 LQ case. The U_1 LQ interaction with the SM fermions is given in Eq. (A1). Integrating the U_1 LQ out, as well as the charged current contributions ($b \to c\tau\bar{\nu}$) in Eq. (A2), the neutral current ones ($b\bar{b} \to \tau^+\tau^-$) are obtained as

$$C^{b\tau}_{VLL}(\mu_{\rm LQ}) = -\frac{|x^{b\tau}_L|^2}{m^2_{U_1}}, \qquad C^{b\tau}_{VRR}(\mu_{\rm LQ}) = -\frac{|x^{b\tau}_R|^2}{m^2_{U_1}},$$
$$C^{b\tau}_{SR}(\mu_{\rm LQ}) = \frac{2x^{b\tau}_L (x^{b\tau}_R)^*}{m^2_{U_1}}. \tag{4.13}$$

The vector contributions do not change under the RGEs, while the scalar contribution does not affect the Υ decay. Here, an important point is that $R_{\Upsilon(3S)}/R^{\rm SM}_{\Upsilon(3S)}$ is predicted to be less than 1 when NP contributions are dominated by vector interactions. It would lead to a coherent deviation with $R_{D^{(*)}}$.

Setting $m_{U_1} = 2.0$ TeV and $(Vx_L(\mu_{\rm LQ}))^{c\tau} = V_{cb}x^{b\tau}_L(\mu_{\rm LQ}) + V_{cs}x^{s\tau}_L(\mu_{\rm LQ})$ with $x^{s\tau}_L/x^{b\tau}_L = \lambda \simeq 0.225$, we show a correlation between $R_{\Upsilon(3S)}$ and $R_{D^{(*)}}$ in Fig. 4. Note

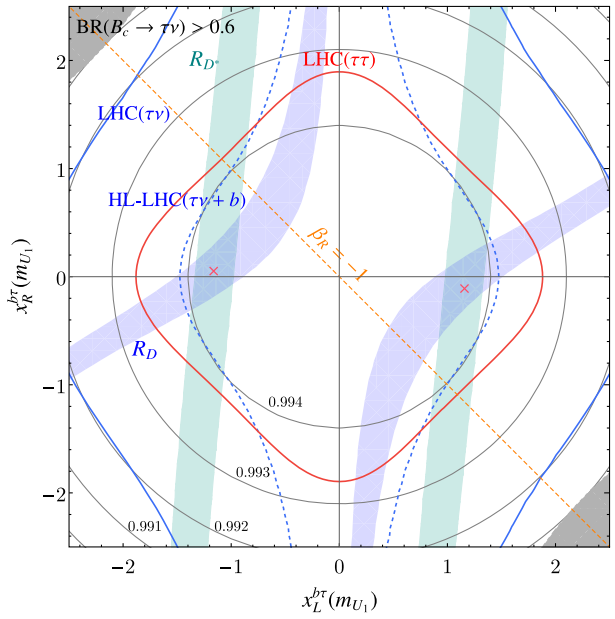

FIG. 4. The correlation between $R_{\Upsilon(3S)}$ and $R_{D^{(*)}}$ is exhibited in the U_1 LQ scenario with $m_{U_1} = 2$ TeV by setting $x^{s\tau}_L/x^{b\tau}_L = \lambda$. The predicted values of $R_{\Upsilon(3S)}$ are shown by black contours. R_D and R_{D^*} anomalies can be explained in the blue and green regions, respectively. The LHC exclusion region from the $\tau +$ missing searches (outside the blue line) and the HL-LHC sensitivity (blue dashed line) are based on the result of Table III. The LHC exclusion region from the nonresonant $\tau^+\tau^-$ searches is shown by the red line. The best-fit points of Eq. (3.12) are shown by red crosses. The orange dashed line represents the $U(2)$ flavor symmetry prediction with $\beta_R = -1$. The gray-shaded region is excluded by the B_c lifetime.

that $x^{s\tau}_L/x^{b\tau}_L = \lambda$ is a typical reference value [166]. Here, favored parameter regions in the U_1 LQ model are exhibited on $x^{b\tau}_L - x^{b\tau}_R$ plane at the renormalization scale $\mu_{\rm LQ} = m_{U_1}$. The black contour represents the expected values of $R_{\Upsilon(3S)}$. It is noted that if we adopt the 2σ constraint of $R^{\rm exp}_{\Upsilon(3S)}$ in Eq. (4.2), the entire parameter region is allowed. The blue and green regions can explain the R_D and R_{D^*} discrepancies within 1σ, respectively. The exclusion region by the LHC analysis ($\tau +$ missing search) is outside the blue line, while the future prospect of the High Luminosity LHC is shown by the blue-dashed line, see Table III. Furthermore, a stronger collider bound comes from a non-resonant $\tau^+\tau^-$ search [100,101], although it is model-parameter dependent. The outside of the red line is excluded by the nonresonant $\tau^+\tau^-$ search, where a public code HIGHPT [220] is used [210]. The orange dashed line stands for a prediction in the case of the UV origin U_1 LQ with $\beta_R = -1(\phi = \pi)$ as a reference value [208]. The gray-shaded region is excluded by the B_c lifetime, i.e., $\mathcal{B}(B_c \to \tau\bar{\nu}) > 0.6$.

From the figure, it is found that the current $R^{\rm exp}_{\Upsilon(3S)}$ overshoots favored parameter region from the $R_{D^{(*)}}$ anomalies. The best-fit points of Eq. (3.12) are shown by red crosses and predict $R_{\Upsilon(3S)} = 0.9942$. Thus, the LFU violation in $R_{\Upsilon(nS)}$ is predicted to be very small in the U_1 LQ scenario.

Next, we investigate the R_2 LQ with $C_{V_R} = 0$ scenario. The R_2 LQ interaction with the SM fermions is given in Eq. (A6). The generated charged current contributions are given in Eq. (A7), while the neutral current one is

$$C^{b\tau}_{VLR}(\mu_{\rm LQ}) = -\frac{|y^{b\tau}_R|^2}{2m^2_{R_2}}. \tag{4.14}$$

Since $C^{b\tau}_{VLR} < 0$, $R_{\Upsilon(3S)}/R^{\rm SM}_{\Upsilon(3S)}$ has to be less than 1 again.

The result is shown in Fig. 5. Here, we set $m_{R_2} = 2.0$ TeV, $y^{c\tau}_L/|y^{b\tau}_R| = 0.7$ with $|V_{cb}| = 0.041$, and take $y^{b\tau}_R(\mu_{\rm LQ})$ as complex value. Note that it is found in Ref. [210] that the choice of $y^{c\tau}_L/|y^{b\tau}_R| \approx 0.7$ can alleviate the bound from the nonresonant $\tau^+\tau^-$ searches. The color convention is the same as the U_1 LQ case. The best-fit points in Eq. (3.16) are shown by red crosses, predicting $R_{\Upsilon(3S)} = 0.9938$. Similar to U_1 LQ interpretation, it seems crucial to measure $R_{\Upsilon(nS)}$ with 0.1% accuracy in order to distinguish the R_2 LQ signal.

Note that the S_1 LQ does not contribute to $R_{\Upsilon(nS)}$, while the V_2 LQ can contribute. However we found that the V_2 contribution is also small; 0.1% effect in $R_{\Upsilon(3S)}$ [163].

At the current stage, the large experimental uncertainty in $R_{\Upsilon(3S)}$ cannot allow a clear-cut conclusion. One should note that the Belle and Belle II experiments have enough sensitivities to the $R_{\Upsilon(nS)}$ measurements, which would be

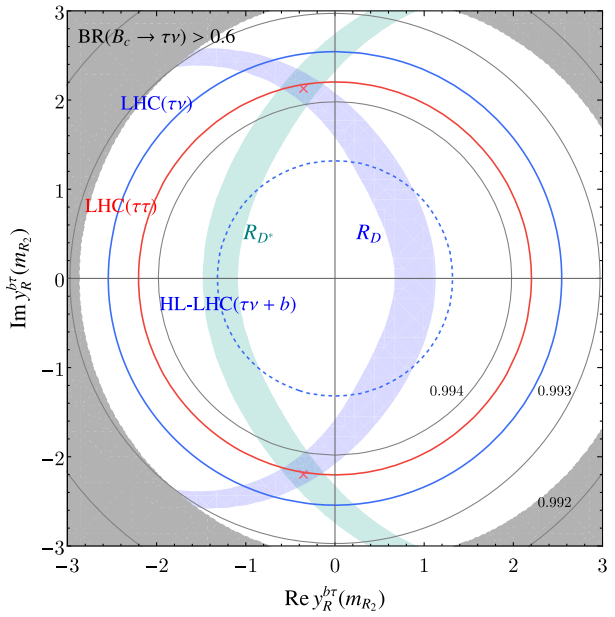

FIG. 5. The correlation between $R_{\Upsilon(3S)}$ and $R_{D^{(*)}}$ in the R_2 LQ scenario with $C_{V_R} = 0$ and $m_{R_2} = 2$ TeV by setting and $y_L^{c\tau}/|y_R^{b\tau}| = 0.7$. The color convention is the same as in Fig. 4. The best-fit points of Eq. (3.16) are shown by red crosses.

more accurate than the existing *BABAR* measurement [221].

V. CONCLUSIONS AND DISCUSSION

In this work, we revisited our previous phenomenological investigation and presented the statistical analysis of the LFU violation in $R_{D^{(*)}}$, including the new experimental data from the LHCb and Belle II experiments. Starting with the reevaluation of the generic formulas for $R_{D^{(*)}}$ by employing the recent development of the $B \to D^{(*)}$ transition form factors, we examined the NP possibility with the low-energy effective Lagrangian as well as the LQ models. In addition to the constraints from the low-energy observables and the high-p_T mono-τ search at LHC, the predictions on the relevant observables of R_Υ, $R_{J/\psi}$, and the τ polarizations $P_\tau^{D^{(*)}}$ are evaluated.

To be precise, we performed the χ^2 fit to the experimental measurements of $R_{D^{(*)}}$ and the D^* polarization $F_L^{D^*}$. This updated analysis shows that the present data deviates from the SM predictions at $\sim 4\sigma$ level. Our fit result is summarized in Table IV with Eqs. (3.3)–(3.6) for the single-operator scenarios, and Table V with Eqs. (3.12)–(3.16) and (3.23) for the single-LQ scenarios. The NP fit improvements compared with the SM one are visualized by Pull as usual, and it is found that the SM-like vector operator still gives the best Pull.

Due to the new LHCb and Belle II results, the experimental world average has slightly come close to the SM predictions of R_D and R_{D^*}. Moreover, the recent $F_L^{D^*}$ result from the LHCb made the experimental value consistent with the SM prediction. These changes altered the previous situations that the scalar and tensor NP solutions to the $b \to c\tau\nu$ anomaly had been disfavored. Namely, the scalar and tensor NP interpretations have been revived now. On the other hand, it is found that the results of the LQ scenarios do not drastically change compared with the previous fit.

As it was pointed out in the literature, the precise measurements of the polarization observables $P_\tau^{D^{(*)}}$ and $F_L^{D^*}$ have the potential to distinguish the NP scenarios. In Figs. 2 and 3, we show our predictions of P_τ^D and $P_\tau^{D^*}$ for the possible NP scenarios. One can make sure that the single-operator NP scenario explaining the $b \to c\tau\nu$ anomaly can be identified by the $P_\tau^{D^{(*)}}$ measurements, which may be available at the Belle II experiment. On the other hand, the general LQ scenarios are hard to be distinguished due to predicting wide ranges of $P_\tau^{D^{(*)}}$. Once the LQ model with restricted interactions is constructed, however, we see that the $P_\tau^{D^{(*)}}$ measurement has significant potential to probe the LQ signature. The high energy collider search is also important since the high-p_T lepton search at the LHC can directly probe the NP interactions affecting the LFU ratios.

We also investigated the NP impacts on the LFU violation in the $\Upsilon(nS)$ decays. We found that the LFU ratio R_Υ is expected to be deviated from the SM prediction by $\mathcal{O}(0.1)\%$ in the U_1, R_2, and V_2 LQ scenarios for the $R_{D^{(*)}}$ anomaly, while S_1 LQ scenarios expect no deviation. Hence, an experimental accuracy of less than 0.1% for the $R_{\Upsilon(nS)}$ measurement is necessary in order to identify the LQ scenario based on the distinct correlation.

In Table VI, we put a summary check sheet to find which single-mediator NP scenarios are viable and to see important observables in order to identify the NP scenario responsible for the $b \to c\tau\nu$ anomaly.

ACKNOWLEDGMENTS

The authors would like to thank Motoi Endo, Akimasa Ishikawa, Satoshi Mishima, Yuta Takahashi, and Kei Yamamoto for fruitful comments and valuable discussion at different stages of the work. We also appreciate Monika Blanke, Andreas Crivellin, Marco Fedele, Ulrich Nierste, and Felix Wilsch for useful discussion. S. I. enjoyed the support from the Deutsche Forschungsgemeinschaft (DFG, German Research Foundation) under Grant No. 396021762-TRR 257. S. I. thanks Karlsruhe House of Young Scientists (KHYS) for the financial support which enabled him to invite R. W. for the discussion. The work of T. K. was supported by the Japan Society for the Promotion of Science (JSPS) Grant-in-Aid for Early-Career Scientists (Grant No. 19K14706). The work of S. I. and T. K. are supported by the JSPS Core-to-Core Program (Grant No. JPJSCCA20200002). R. W. was partially supported

by the INFN grant "FLAVOR" and the PRIN 2017L5W2PT.

APPENDIX: LEPTOQUARK INTERACTIONS

The LQ interactions are classified with the generic $SU(3)_c \times SU(2)_L \times U(1)_Y$ invariant form [222]. We leave details of the model constructions and then just introduce the interactions relevant for $b \to c\tau\bar{\nu}$. As mentioned above, there are four viable candidates of LQs: U_1, S_1, R_2 [223], and V_2 [163]. Their quantum numbers under $SU(3)_C$, $SU(2)_L$, $U(1)_Y$ are summarized in Table VI.

First, the U_1 vector LQ interaction with the SM fermions, defined in the interaction basis, is given by

$$\mathcal{L}_{U_1} = x_L^{ij}\bar{Q}_i\gamma_\mu U_1^\mu L_j + x_R^{ij}\bar{d}_{Ri}\gamma_\mu U_1^\mu \ell_{Rj} + \text{H.c.} \tag{A1}$$

Integrating out the U_1 LQ mediator particle, then, the WCs for the charged current of our interest ($b \to c\tau\bar{\nu}$) is obtained as

$$C_{V_L}(\mu_{\rm LQ}) = \frac{1}{2\sqrt{2}G_F V_{cb}}\frac{(Vx_L)^{c\tau}(x_L^{b\tau})^*}{m_{U_1}^2},$$
$$C_{S_R}(\mu_{\rm LQ}) = -\frac{1}{\sqrt{2}G_F V_{cb}}\frac{(Vx_L)^{c\tau}(x_R^{b\tau})^*}{m_{U_1}^2}, \tag{A2}$$

where V is the CKM matrix and the couplings $x_{L,R}$ are in the mass basis. The relative sign and factor two in Eq. (A2) come from the property of Fierz identity.

In a typical UV completed theory [208], the U_1 LQ is realized as a gauge boson generated from a large gauge symmetry and only couples to the third-generation SM fermions. Namely, $x_R^{b\tau} = x_L^{b\tau} \equiv g_U$, with the others to be zero, is indicated in the gauge interaction basis. Moving to the mass basis, then, generates a nonzero off-diagonal part such as $x_L^{c\tau}$ and also $x_R^{b\tau} = e^{-i\phi}x_L^{b\tau}$, where the phase comes from those in the rotation matrices to the mass bases of the left- and right-handed quark and lepton fields that are not canceled in general. Therefore, the UV completion of U_1 LQ suggests

$$C_{S_R}(\mu_{\rm LQ}) = -2e^{i\phi}C_{V_L}(\mu_{\rm LQ}), \tag{A3}$$

as introduced in the main text. We also comment that an extension of the fermion families with a nontrivial texture of the fermion mass matrices is necessary to construct a practical UV model [178].

The S_1 scalar LQ interaction in the mass basis is given by

$$\mathcal{L}_{S_1} = (V^* y_L)^{ij}\overline{u_{Li}^C}\ell_{Lj}S_1 - y_L^{ij}\overline{d_{Li}^C}\nu_{Lj}S_1 + y_R^{ij}\overline{u_{Ri}^C}\ell_{Rj}S_1 + \text{H.c.} \tag{A4}$$

In the scalar LQ scenario, the source of the generation violating couplings is off-diagonal element of Yukawa matrices. Then the four-fermion interactions of $b \to c\tau\bar{\nu}$ are given by

$$C_{S_L}(\mu_{\rm LQ}) = -4C_T(\mu_{\rm LQ}) = -\frac{1}{4\sqrt{2}G_F V_{cb}}\frac{y_L^{b\tau}(y_R^{c\tau})^*}{m_{S_1}^2},$$
$$C_{V_L}(\mu_{\rm LQ}) = \frac{1}{4\sqrt{2}G_F V_{cb}}\frac{y_L^{b\tau}(Vy_L^*)^{c\tau}}{m_{S_1}^2}. \tag{A5}$$

We also introduce the R_2 scalar LQ interaction. R_2 is a SU(2) doublet and a component with 2/3 of the electromagnetic charge $R_2^{(2/3)}$ can contribute to $b \to c\tau\bar{\nu}$. The Yukawa interaction

$$\mathcal{L}_{R_2} = y_R^{ij}\bar{d}_{Li}\ell_{Rj}R_2^{(2/3)} + y_L^{ij}\bar{u}_{Ri}\nu_{Lj}R_2^{(2/3)} + \text{H.c.}, \tag{A6}$$

gives

$$C_{S_L}(\mu_{\rm LQ}) = 4C_T(\mu_{\rm LQ}) = \frac{1}{4\sqrt{2}G_F V_{cb}}\frac{y_L^{c\tau}(y_R^{b\tau})^*}{m_{R_2}^2}. \tag{A7}$$

In contrast to the above two LQ scenarios, the R_2 LQ does not generate C_{V_L} but C_{V_R}. Thus we could expect solid predictions in polarization and related observables. To generate C_{V_R}, indeed, a large mixing between two distinct R_2 LQ doublet is required to induce a proper electroweak symmetry breaking. See details in Refs. [98,117].

TABLE VI. Summary table for the single-mediator NP scenarios in light of the $b \to c\tau\nu$ anomaly. We add implications for the LHC searches and flavor observables in the last two columns, which is useful to identify the NP scenario. In the $V_2^{(1/3)}$ LQ scenario, 2σ for R_{D^*} implies that it can explain the R_{D^*} anomaly within the 2σ range (but not within 1σ).

	Spin	Charge	Operators	R_D	R_{D^*}	LHC	Flavor
$H^\pm$	0	$(\mathbf{1},\mathbf{2},1/2)$	O_{S_L}	✓	✓	$b\tau\nu$	$B_c \to \tau\nu$, $F_L^{D^*}$, $P_\tau^{D^*}$, M_W
S_1	0	$(\bar{\mathbf{3}},\mathbf{1},1/3)$	O_{V_L}, O_{S_L}, O_T	✓	✓	$\tau\tau$	ΔM_s, P_τ^D, $B \to K^{(*)}\nu\nu$
$R_2^{(2/3)}$	0	$(\mathbf{3},\mathbf{2},7/6)$	O_{S_L}, O_T, (O_{V_R})	✓	✓	$b\tau\nu$, $\tau\tau$	$P_\tau^{D^*}$, M_W, $Z \to \tau\tau$, d_N
U_1	1	$(\mathbf{3},\mathbf{1},2/3)$	O_{V_L}, O_{S_R}	✓	✓	$b\tau\nu$, $\tau\tau$	ΔM_s, $R_{K^{(*)}}$, $B_s \to \tau\tau$, d_N
$V_2^{(1/3)}$	1	$(\bar{\mathbf{3}},\mathbf{2},5/6)$	O_{S_R}	✓	2σ	$\tau\tau$	$B_s \to \tau\tau$, $B_u \to \tau\nu$, M_W

Finally, we introduce the isodoublet vector V_2 LQ. A component with electromagnetic charge of 1/3, $V_2^{(1/3)}$, contributes to $b \to c\tau\bar{\nu}$. The interaction Lagrangian in the interaction basis is given by

$$\mathcal{L}_{V_2} = -z_L^{ij}(\overline{d_{Ri}^C}\gamma_\mu \nu_{Lj})V_2^{(1/3),\mu} + (V^* z_R)^{ij}(\overline{u_{Li}^C}\gamma_\mu \ell_{Rj})V_2^{(1/3),\mu} + \text{H.c.}, \quad \text{(A8)}$$

where indices i, j are labels of flavor. Integrating out the V_2 gives

$$C_{S_R} = -\frac{1}{\sqrt{2}G_F V_{cb}}\frac{z_L^{b\tau}(V z_R^*)^{c\tau}}{m_{V_2}^2}. \quad \text{(A9)}$$

It is noted that although the U_1 LQ scenario also contributes to C_{S_R}, the scenario can have C_{V_L} solely so that the $R_{D^{(*)}}$ anomaly can be explained. Furthermore, the isospin partner $V_2^{(4/3)}$ provides distinct model predictions compared to the U_1 LQ scenario [163].

[1] *BABAR* Collaboration, Evidence for an excess of $\bar{B} \to D^{(*)}\tau^-\bar{\nu}_\tau$ decays, Phys. Rev. Lett. **109**, 101802 (2012).

[2] *BABAR* Collaboration, Measurement of an excess of $\bar{B} \to D^{(*)}\tau^-\bar{\nu}_\tau$ decays and implications for charged Higgs bosons, Phys. Rev. D **88**, 072012 (2013).

[3] LHCb Collaboration, Measurement of the ratio of branching fractions $\mathcal{B}(\bar{B}^0 \to D^{*+}\tau^-\bar{\nu}_\tau)/\mathcal{B}(\bar{B}^0 \to D^{*+}\mu^-\bar{\nu}_\mu)$, Phys. Rev. Lett. **115**, 111803 (2015); **115**, 159901(E) (2015).

[4] LHCb Collaboration, Measurement of the ratio of the $B^0 \to D^{*-}\tau^+\nu_\tau$ and $B^0 \to D^{*-}\mu^+\nu_\mu$ branching fractions using three-prong τ-lepton decays, Phys. Rev. Lett. **120**, 171802 (2018).

[5] LHCb Collaboration, Test of lepton flavor universality by the measurement of the $B^0 \to D^{*-}\tau^+\nu_\tau$ branching fraction using three-prong τ decays, Phys. Rev. D **97**, 072013 (2018).

[6] LHCb Collaboration, Measurement of the ratios of branching fractions $\mathcal{R}(D^*)$ and $\mathcal{R}(D^0)$, Phys. Rev. Lett. **131**, 111802 (2023).

[7] Belle Collaboration, Measurement of the branching ratio of $\bar{B} \to D^{(*)}\tau^-\bar{\nu}_\tau$ relative to $\bar{B} \to D^{(*)}\ell^-\bar{\nu}_\ell$ decays with hadronic tagging at Belle, Phys. Rev. D **92**, 072014 (2015).

[8] Belle Collaboration, Measurement of the τ lepton polarization and $R(D^*)$ in the decay $\bar{B} \to D^*\tau^-\bar{\nu}_\tau$, Phys. Rev. Lett. **118**, 211801 (2017).

[9] Belle Collaboration, Measurement of the τ lepton polarization and $R(D^*)$ in the decay $\bar{B} \to D^*\tau^-\bar{\nu}_\tau$ with one-prong hadronic τ decays at Belle, Phys. Rev. D **97**, 012004 (2018).

[10] Belle Collaboration, Measurement of $\mathcal{R}(D)$ and $\mathcal{R}(D^*)$ with a semileptonic tagging method, arXiv:1904.08794.

[11] Belle Collaboration, Measurement of $\mathcal{R}(D)$ and $\mathcal{R}(D^*)$ with a semileptonic tagging method, Phys. Rev. Lett. **124**, 161803 (2020).

[12] Belle-II Collaboration, First flavor tagging calibration using 2019 Belle II data, arXiv:2008.02707.

[13] Belle-II Collaboration, A test of lepton flavor universality with a measurement of $R(D^*)$ using hadronic B tagging at the Belle II experiment, arXiv:2401.02840.

[14] HFLAV Collaboration, Preliminary average of $R(D)$ and $R(D^*)$ for Moriond 2024, https://hflav-eos.web.cern.ch/hflav-eos/semi/moriond24/html/RDsDsstar/RDRDs.html.

[15] LHCb Collaboration, $R(D^*)$ and $R(D)$ with $\tau^- \to \mu^-\nu_\tau\bar{\nu}_\mu$, https://indico.cern.ch/event/1187939/.

[16] LHCb Collaboration, Measurement of $R(D^*)$ with hadronic τ^+ decays at $\sqrt{s} = 13$ TeV by the LHCb collaboration, https://indico.cern.ch/event/1231797/.

[17] LHCb Collaboration, Test of lepton flavor universality using $B^0 \to D^{*-}\tau^+\nu_\tau$ decays with hadronic τ channels, Phys. Rev. D **108**, 012018 (2023).

[18] Belle II Collaboration, Recent Belle II results on semileptonic B decays and tests of lepton-flavor universality, https://indico.cern.ch/event/1114856/contributions/5423684/.

[19] LHCb Collaboration, $b \to cl\nu$ decays at LHCb, https://indico.in2p3.fr/event/32664/timetable/?view=standard_numbered#38-b-to-c-l-nu-decays-at-lhcb.

[20] D. London and J. Matias, B flavour anomalies: 2021 Theoretical status report, Annu. Rev. Nucl. Part. Sci. **72**, 37 (2022).

[21] B. Capdevila, A. Crivellin, and J. Matias, Review of semileptonic B anomalies, Eur. Phys. J. Spec. Top. **1**, 20 (2023).

[22] Belle-II Collaboration, Snowmass white paper: Belle II physics reach and plans for the next decade and beyond, arXiv:2207.06307.

[23] G. Landsberg, B physics parking program in CMS, in *Proceedings of the 20th Annual RDMS CMS Collaboration Conference* https://indico.cern.ch/event/754760/contributions/3127694/ (2018).

[24] CMS Collaboration, Recording and reconstructing 10 billion unbiased b hadron decays in CMS, https://cds.cern.ch/record/2704495 (2019).

[25] R. Bainbridge, Recording and reconstructing 10 billion unbiased b hadron decays in CMS, EPJ Web Conf. **245**, 01025 (2020).

[26] Y. Takahashi, Indications of new physics beyond the Standard Model in flavor anomalies observed at the LHC experiments, in *The Physical Society of Japan 2020 Autumn Meeting* (2020).

[27] Heavy Flavor Averaging Group and HFLAV Collaborations, Averages of b-hadron, c-hadron, and τ-lepton properties as of 2021, Phys. Rev. D **107**, 052008 (2023); , Average of R_D and R_{D^*} for Spring 2021, https://hflav-eos.web.cern.ch/hflav-eos/semi/spring21/html/RDsDsstar/RDRDs.html.

[28] F. U. Bernlochner, M. F. Sevilla, D. J. Robinson, and G. Wormser, Semitauonic b-hadron decays: A lepton flavor universality laboratory, Rev. Mod. Phys. **94**, 015003 (2022).

[29] F. U. Bernlochner, Z. Ligeti, M. Papucci, M. T. Prim, Dean J. Robinson, and C. Xiong, Constrained second-order power corrections in HQET: $R(D^{(*)})$, $|V_{cb}|$, and new physics, Phys. Rev. D **106**, 096015 (2022).

[30] S. Iguro and R. Watanabe, Bayesian fit analysis to full distribution data of $\bar{\mathrm{B}} \to \mathrm{D}^{(*)}\ell\bar{\nu}$: $|\mathrm{V_{cb}}|$ determination and new physics constraints, J. High Energy Phys. 08 (2020) 006.

[31] M. Bordone, M. Jung, and D. van Dyk, Theory determination of $\bar{B} \to D^{(*)}\ell^-\bar{\nu}$ form factors at $\mathcal{O}(1/m_c^2)$, Eur. Phys. J. C **80**, 74 (2020).

[32] M. Bordone, N. Gubernari, D. van Dyk, and M. Jung, Heavy-quark expansion for $\bar{B}_s \to D_s^{(*)}$ form factors and unitarity bounds beyond the $SU(3)_F$ limit, Eur. Phys. J. C **80**, 347 (2020).

[33] D. Bigi and P. Gambino, Revisiting $B \to D\ell\nu$, Phys. Rev. D **94**, 094008 (2016).

[34] F. U. Bernlochner, Z. Ligeti, M. Papucci, and D. J. Robinson, Combined analysis of semileptonic B decays to D and D^*: $R(D^{(*)})$, $|V_{cb}|$, and new physics, Phys. Rev. D **95**, 115008 (2017); **97**, 059902(E) (2018).

[35] S. Jaiswal, S. Nandi, and S. K. Patra, Extraction of $|V_{cb}|$ from $B \to D^{(*)}\ell\nu_\ell$ and the standard model predictions of $R(D^{(*)})$, J. High Energy Phys. 12 (2017) 060.

[36] P. Gambino, M. Jung, and S. Schacht, The V_{cb} puzzle: An update, Phys. Lett. B **795**, 386 (2019).

[37] *BABAR* Collaboration, Extraction of form Factors from a Four-Dimensional Angular Analysis of $\bar{B} \to D^*\ell^-\bar{\nu}_\ell$, Phys. Rev. Lett. **123**, 091801 (2019).

[38] G. Martinelli, S. Simula, and L. Vittorio, $|V_{cb}|$ and $R(D)^{(*)}$ using lattice QCD and unitarity, Phys. Rev. D **105**, 034503 (2022).

[39] Fermilab Lattice and MILC Collaborations, Semileptonic form factors for $B \to D^*\ell\nu$ at nonzero recoil from $2+1$-flavor lattice QCD, Eur. Phys. J. C **82**, 1141 (2022); **83**, 21 (E) (2023).

[40] JLQCD Collaboration, $B \to D^*\ell\nu_\ell$ semileptonic form factors from lattice QCD with Möbius domain-wall quarks, Phys. Rev. D **109**, 074503 (2024).

[41] J. Harrison and C. T. H. Davies, $B \to D^*$ vector, axial-vector and tensor form factors for the full q^2 range from lattice QCD, Phys. Rev. D **109**, 094515 (2024).

[42] E. McLean, C. T. H. Davies, J. Koponen, and A. T. Lytle, $B_s \to D_s\ell\nu$ form factors for the full q^2 range from Lattice QCD with non-perturbatively normalized currents, Phys. Rev. D **101**, 074513 (2020).

[43] LATTICE-HPQCD Collaboration, $R(J/\psi)$ and $B_c^- \to J/\psi\ell^-\bar{\nu}_\ell$ lepton flavor universality violating observables from lattice QCD, Phys. Rev. Lett. **125**, 222003 (2020).

[44] F. U. Bernlochner, Z. Ligeti, D. J. Robinson, and W. L. Sutcliffe, New predictions for $\Lambda_b \to \Lambda_c$ semileptonic decays and tests of heavy quark symmetry, Phys. Rev. Lett. **121**, 202001 (2018).

[45] D. Aloni, A. Efrati, Y. Grossman, and Y. Nir, Υ and ψ leptonic decays as probes of solutions to the $R_D^{(*)}$ puzzle, J. High Energy Phys. 06 (2017) 019.

[46] S. de Boer, T. Kitahara, and I. Nisandzic, Soft-photon corrections to $\bar{B} \to D\tau^-\bar{\nu}_\tau$ relative to $\bar{B} \to D\mu^-\bar{\nu}_\mu$, Phys. Rev. Lett. **120**, 261804 (2018).

[47] S. Calí, S. Klaver, M. Rotondo, and B. Sciascia, Impacts of radiative corrections on measurements of lepton flavour universality in $B \to D\ell\nu_\ell$ decays, Eur. Phys. J. C **79**, 744 (2019).

[48] G. Isidori and O. Sumensari, Optimized lepton universality tests in $B \to V\ell\bar{\nu}$ decays, Eur. Phys. J. C **80**, 1078 (2020).

[49] M. Papucci, T. Trickle, and M. B. Wise, Radiative semileptonic $\bar{B}$ decays, J. High Energy Phys. 02 (2022) 043.

[50] M. Tanaka and R. Watanabe, Tau longitudinal polarization in $B \to D\tau\nu$ and its role in the search for charged Higgs boson, Phys. Rev. D **82**, 034027 (2010).

[51] Y. Sakaki and H. Tanaka, Constraints on the charged scalar effects using the forward-backward asymmetry on $\mathrm{B}^- \to \mathrm{D}(*)\tau\nu^-\tau$, Phys. Rev. D **87**, 054002 (2013).

[52] M. Duraisamy and A. Datta, The full $B \to D^*\tau^-\overline{\nu_\tau}$ angular distribution and CP violating triple products, J. High Energy Phys. 09 (2013) 059.

[53] M. Duraisamy, P. Sharma, and A. Datta, Azimuthal $B \to D^*\tau^-\overline{\nu_\tau}$ angular distribution with tensor operators, Phys. Rev. D **90**, 074013 (2014).

[54] D. Becirevic, S. Fajfer, I. Nisandzic, and A. Tayduganov, Angular distributions of $\overline{B} \to D^{(*)}\ell\bar{\nu}_\ell$ decays and search of new physics, Nucl. Phys. **B946**, 114707 (2019).

[55] A. K. Alok, D. Kumar, S. Kumbhakar, and S. U. Sankar, D^* polarization as a probe to discriminate new physics in $\bar{B} \to D^*\tau\bar{\nu}$, Phys. Rev. D **95**, 115038 (2017).

[56] M. A. Ivanov, J. G. Körner, and C.-T. Tran, Probing new physics in $\bar{B}^0 \to D^{(*)}\tau^-\bar{\nu}_\tau$ using the longitudinal, transverse, and normal polarization components of the tau lepton, Phys. Rev. D **95**, 036021 (2017).

[57] P. Colangelo and F. De Fazio, Scrutinizing $\bar{B} \to D^*(D\pi)\ell^-\bar{\nu}_\ell$ and $\bar{B} \to D^*(D\gamma)\ell^-\bar{\nu}_\ell$ in search of new physics footprints, J. High Energy Phys. 06 (2018) 082.

[58] S. Bhattacharya, S. Nandi, and S. Kumar Patra, $b \to c\tau\nu_\tau$ decays: A catalogue to compare, constrain, and correlate new physics effects, Eur. Phys. J. C **79**, 268 (2019).

[59] S. Iguro, T. Kitahara, Y. Omura, R. Watanabe, and K. Yamamoto, D^* polarization vs. $R_{D^{(*)}}$ anomalies in the leptoquark models, J. High Energy Phys. 02 (2019) 194.

[60] M. Blanke, A. Crivellin, S. de Boer, M. Moscati, U. Nierste, I. Nišandžić, and T. Kitahara, Impact of polarization observables and $B_c \to \tau\nu$ on new physics explanations of the $b \to c\tau\nu$ anomaly, Phys. Rev. D **99**, 075006 (2019).

[61] M. Blanke, A. Crivellin, T. Kitahara, M. Moscati, U. Nierste, and I. Nišandžić, Addendum to: Impact of polarization observables and $B_c \to \tau\nu$ on new physics explanations of the $b \to c\tau\nu$ anomaly, Phys. Rev. D **100**, 035035(A) (2019).

[62] D. Bečirević, M. Fedele, I. Nišandžić, and A. Tayduganov, Lepton flavor universality tests through angular observables of $\bar{B} \to D^{(*)}\ell\bar{\nu}$ decay modes, arXiv:1907.02257.

[63] D. Hill, M. John, W. Ke, and A. Poluektov, Model-independent method for measuring the angular coefficients of $B^0 \to D^{*-}\tau^+\nu_\tau$ decays, J. High Energy Phys. 11 (2019) 133.

[64] M. Algueró, S. Descotes-Genon, J. Matias, and M. Novoa-Brunet, Symmetries in $B \to D^*\ell\nu$ angular observables, J. High Energy Phys. 06 (2020) 156.

[65] B. Bhattacharya, A. Datta, S. Kamali, and D. London, A measurable angular distribution for $\bar{B} \to D^*\tau^-\bar{\nu}_\tau$ decays, J. High Energy Phys. 07 (2020) 194.

[66] N. Penalva, E. Hernández, and J. Nieves, New physics and the tau polarization vector in $b \to c\tau\bar{\nu}_\tau$ decays, J. High Energy Phys. 06 (2021) 118.

[67] N. Penalva, E. Hernández, and J. Nieves, Visible energy and angular distributions of the charged particle from the τ-decay in $b \to c\tau(\mu\bar{\nu}_\mu\nu_\tau, \pi\nu_\tau, \rho\nu_\tau)\bar{\nu}_\tau$ reactions, J. High Energy Phys. 04 (2022) 026.

[68] M. Tanaka and R. Watanabe, New physics in the weak interaction of $\bar{B} \to D^{(*)}\tau\bar{\nu}$, Phys. Rev. D **87**, 034028 (2013).

[69] P. Asadi, M. R. Buckley, and D. Shih, Asymmetry observables and the origin of $R_{D^{(*)}}$ anomalies, Phys. Rev. D **99**, 035015 (2019).

[70] Belle Collaboration, Measurement of the D^{*-} polarization in the decay $B^0 \to D^{*-}\tau^+\nu_\tau$, arXiv:1903.03102.

[71] LHCb Collaboration, LHCb measurements on semileptonic decays of b-hadrons, https://cds.cern.ch/record/2868260.

[72] LHCb Collaboration, Measurement of the D^* longitudinal polarization in $B^0 \to D^{*-}\tau^+\nu_\tau$ decays, arXiv:2311.05224.

[73] Belle Collaboration, Measurement of differential distributions of $B \to D^*\ell\bar{\nu}_\ell$ and implications on $|V_{cb}|$, Phys. Rev. D **108**, 012002 (2023).

[74] Belle-II Collaboration, Determination of $|V_{cb}|$ using $\bar{B}^0 \to D^{*+}\ell^-\bar{\nu}_\ell$ decays with Belle II, Phys. Rev. D **108**, 092013 (2023).

[75] M. Fedele, M. Blanke, A. Crivellin, S. Iguro, U. Nierste, S. Simula, and L. Vittorio, Discriminating $B \to D^*\ell\nu$ form factors via polarization observables and asymmetries, Phys. Rev. D **108**, 055037 (2023).

[76] Belle II Collaboration, Recent Belle II results on semi-tauonic decays and tests of lepton-flavor universality, https://indico.desy.de/event/34916/contributions/146854.

[77] Belle-II Collaboration, First measurement of $R(X_{\tau/\ell})$ as an inclusive test of the $b \to c\tau\nu$ anomaly, Phys. Rev. Lett. **132**, 211804 (2024).

[78] M. Freytsis, Z. Ligeti, and J. T. Ruderman, Flavor models for $\bar{B} \to D^{(*)}\tau\bar{\nu}$, Phys. Rev. D **92**, 054018 (2015).

[79] Z. Ligeti, M. Luke, and F. J. Tackmann, Theoretical predictions for inclusive $B \to X_u\tau\nu^-$ decay, Phys. Rev. D **105**, 073009 (2022).

[80] M. Rahimi and K. K. Vos, Standard model predictions for lepton flavour universality ratios of inclusive semileptonic B decays, J. High Energy Phys. 11 (2022) 007.

[81] ALEPH Collaboration, Measurements of $\mathrm{BR}(b \to \tau^-\bar{\nu}_\tau X)$ and $\mathrm{BR}(b \to \tau^-\bar{\nu}_\tau D^{*\pm}X)$ and upper limits on $\mathrm{BR}(B^- \to \tau^-\bar{\nu}_\tau)$ and $\mathrm{BR}(b \to s\nu\bar{\nu})$, Eur. Phys. J. C **19**, 213 (2001).

[82] A. Celis, M. Jung, X.-Q. Li, and A. Pich, Scalar contributions to $b \to c(u)\tau\nu$ transitions, Phys. Lett. B **771**, 168 (2017).

[83] S. Kamali, New physics in inclusive semileptonic B decays including nonperturbative corrections, Int. J. Mod. Phys. A **34**, 1950036 (2019).

[84] M. Jung and D. M. Straub, Constraining new physics in $b \to c\ell\nu$ transitions, J. High Energy Phys. 01 (2019) 009.

[85] G. Martinelli, S. Simula, and L. Vittorio, Updates on the determination of $|V_{cb}|$, $R(D^*)$ and $|V_{ub}|/|V_{cb}|$, Eur. Phys. J. C **84**, 400 (2024).

[86] T. Kapoor, Z.-R. Huang, and E. Kou, New physics search via angular distribution of $B \to D^*\ell\nu_\ell$ decay in the light of the new lattice data, arXiv:2401.11636.

[87] G. Martinelli, S. Simula, and L. Vittorio, Constraints for the semileptonic $B \to D(*)$ form factors from lattice QCD simulations of two-point correlation functions, Phys. Rev. D **104**, 094512 (2021).

[88] G. Martinelli, S. Simula, and L. Vittorio, Exclusive determinations of $|V_{cb}|$ and $R(D^*)$ through unitarity, Eur. Phys. J. C **82**, 1083 (2022).

[89] A. Greljo, J. Martin Camalich, and J. D. Ruiz-Álvarez, Mono-τ signatures at the LHC constrain explanations of B-decay anomalies, Phys. Rev. Lett. **122**, 131803 (2019).

[90] B. Dumont, K. Nishiwaki, and R. Watanabe, LHC constraints and prospects for S_1 scalar leptoquark explaining the $\bar{B} \to D^{(*)}\tau\bar{\nu}$ anomaly, Phys. Rev. D **94**, 034001 (2016).

[91] W. Altmannshofer, P. S. Bhupal Dev, and A. Soni, $R_{D^{(*)}}$ anomaly: A possible hint for natural supersymmetry with R-parity violation, Phys. Rev. D **96**, 095010 (2017).

[92] S. Iguro and K. Tobe, $R(D^{(*)})$ in a general two Higgs doublet model, Nucl. Phys. **B925**, 560 (2017).

[93] M. Abdullah, J. Calle, B. Dutta, A. Flórez, and D. Restrepo, Probing a simplified, W' model of $R(D^{(*)})$ anomalies using b-tags, τ leptons and missing energy, Phys. Rev. D **98**, 055016 (2018).

[94] S. Iguro, Y. Omura, and M. Takeuchi, Test of the $R(D^{(*)})$ anomaly at the LHC, Phys. Rev. D **99**, 075013 (2019).

[95] M. J. Baker, J. Fuentes-Martín, G. Isidori, and M. König, High- p_T signatures in vector–leptoquark models, Eur. Phys. J. C **79**, 334 (2019).

[96] D. Marzocca, U. Min, and M. Son, Bottom-flavored mono-tau tails at the LHC, J. High Energy Phys. 12 (2020) 035.

[97] S. Iguro, M. Takeuchi, and R. Watanabe, Testing leptoquark/EFT in $\bar{B} \to D^{(*)}l\bar{\nu}$ at the LHC, Eur. Phys. J. C **81**, 406 (2021).

[98] M. Endo, S. Iguro, T. Kitahara, M. Takeuchi, and R. Watanabe, Non-resonant new physics search at the LHC for the $b \to c\tau\nu$ anomalies, J. High Energy Phys. 02 (2022) 106.

[99] F. Jaffredo, Revisiting mono-tau tails at the LHC, Eur. Phys. J. C **82**, 541 (2022).

[100] ATLAS Collaboration, Search for heavy Higgs bosons decaying into two tau leptons with the ATLAS detector using pp collisions at $\sqrt{s} = 13$ TeV, Phys. Rev. Lett. **125**, 051801 (2020).

[101] CMS Collaboration, Searches for additional Higgs bosons and for vector leptoquarks in $\tau\tau$ final states in proton-proton collisions at $\sqrt{s} = 13$ TeV, J. High Energy Phys. 07 (2023) 073.

[102] LHCb Collaboration, Measurement of the ratio of branching fractions $\mathcal{B}(B_c^+ \to J/\psi\tau^+\nu_\tau)/\mathcal{B}(B_c^+ \to J/\psi\mu^+\nu_\mu)$, Phys. Rev. Lett. **120**, 121801 (2018).

[103] CMS Collaboration, Recent CMS results on flavor anomalies and lepton flavor violation, https://indico.desy.de/event/34916/contributions/146862/.

[104] CMS Collaboration, Lepton flavour (universality) violation studies at CMS, https://indico.cern.ch/event/1291157/contributions/5878345/.

[105] *BABAR* Collaboration, Precision measurement of the $\mathcal{B}(\Upsilon(3S) \to \tau^+\tau^-)/\mathcal{B}(\Upsilon(3S) \to \mu^+\mu^-)$ ratio, Phys. Rev. Lett. **125**, 241801 (2020).

[106] Y. Sakaki, M. Tanaka, A. Tayduganov, and R. Watanabe, Testing leptoquark models in $\bar{B} \to D^{(*)}\tau\bar{\nu}$, Phys. Rev. D **88**, 094012 (2013).

[107] Z.-R. Huang, Y. Li, C.-D. Lu, M. A. Paracha, and C. Wang, Footprints of new physics in $b \to c\tau\nu$ transitions, Phys. Rev. D **98**, 095018 (2018).

[108] E. Kou and P. Urquijo, The Belle II physics book, Prog. Theor. Exp. Phys. **2019**, 123C01 (2019); **2020**, 029201(E) (2020).

[109] S. Iguro and Y. Omura, Status of the semileptonic B decays and muon g-2 in general 2HDMs with right-handed neutrinos, J. High Energy Phys. 05 (2018) 173.

[110] P. Asadi, M. R. Buckley, and D. Shih, It's all right(-handed neutrinos): A new W' model for the $R_{D^{(*)}}$ anomaly, J. High Energy Phys. 09 (2018) 010.

[111] A. Greljo, D. J. Robinson, B. Shakya, and J. Zupan, $R(D^{(*)})$ from W' and right-handed neutrinos, J. High Energy Phys. 09 (2018) 169.

[112] D. J. Robinson, B. Shakya, and J. Zupan, Right-handed neutrinos and $R(\mathrm{D}^{(*)})$, J. High Energy Phys. 02 (2019) 119.

[113] K. S. Babu, B. Dutta, and R. N. Mohapatra, A theory of $R(D^*, D)$ anomaly with right-handed currents, J. High Energy Phys. 01 (2019) 168.

[114] R. Mandal, C. Murgui, A. Peñuelas, and A. Pich, The role of right-handed neutrinos in $b \to c\tau\bar{\nu}$ anomalies, J. High Energy Phys. 08 (2020) 022.

[115] N. Penalva, E. Hernández, and J. Nieves, The role of right-handed neutrinos in $b \to c_\tau(\pi\nu_\tau, \rho\nu_\tau, \mu\bar{\nu}_\mu\nu_\tau)\bar{\nu}_\tau$ from visible final-state kinematics, J. High Energy Phys. 10 (2021) 122.

[116] S. Iguro, S. Mishima, and M. Endo (private communication).

[117] P. Asadi, New solutions to the charged current B-anomalies, Ph.D. thesis, Rutgers University, Piscataway (main), 2019, 10.7282/t3-yhaa-dm09.

[118] Y. Sakaki, M. Tanaka, A. Tayduganov, and R. Watanabe, Probing new physics with q^2 distributions in $\bar{B} \to D^{(*)}\tau\bar{\nu}$, Phys. Rev. D **91**, 114028 (2015).

[119] I. Caprini, L. Lellouch, and M. Neubert, Dispersive bounds on the shape of $\bar{B} \to D^{(*)}\ell\bar{\nu}$ form factors, Nucl. Phys. **B530**, 153 (1998).

[120] F. Feruglio, P. Paradisi, and O. Sumensari, Implications of scalar and tensor explanations of $R_{D^{(*)}}$, J. High Energy Phys. 11 (2018) 191.

[121] D. Bigi, P. Gambino, and S. Schacht, $R(D^*)$, $|V_{cb}|$, and the heavy quark symmetry relations between form factors, J. High Energy Phys. 11 (2017) 061.

[122] M. Beneke and G. Buchalla, The B_c meson lifetime, Phys. Rev. D **53**, 4991 (1996).

[123] R. Alonso, B. Grinstein, and J. Martin Camalich, Lifetime of B_c^- constrains explanations for anomalies in $B \to D^{(*)}\tau\nu$, Phys. Rev. Lett. **118**, 081802 (2017).

[124] R. Watanabe, New physics effect on $B_c \to J/\psi\tau\bar{\nu}$ in relation to the $R_{D^{(*)}}$ anomaly, Phys. Lett. B **776**, 5 (2018).

[125] J. Aebischer and B. Grinstein, Standard model prediction of the B_c lifetime, J. High Energy Phys. 07 (2021) 130.

[126] Particle Data Group, Review of particle physics, Prog. Theor. Exp. Phys. **2020**, 083C01 (2020).

[127] A. G. Akeroyd and C.-H. Chen, Constraint on the branching ratio of $B_c \to \tau\bar{\nu}$ from LEP1 and consequences for $R(D^{(*)})$ anomaly, Phys. Rev. D **96**, 075011 (2017).

[128] D. Bardhan and D. Ghosh, B -meson charged current anomalies: The post-Moriond 2019 status, Phys. Rev. D **100**, 011701 (2019).

[129] T. Zheng, J. Xu, L. Cao, D. Yu, W. Wang, S. Prell, Y.-K. E. Cheung, and M. Ruan, Analysis of $B_c \to \tau\nu_\tau$ at CEPC, Chin. Phys. C **45**, 023001 (2021).

[130] Y. Amhis, M. Hartmann, C. Helsens, D. Hill, and O. Sumensari, Prospects for B_c^+ $\tau^+\nu_\tau$ at FCC-ee, J. High Energy Phys. 12 (2021) 133.

[131] X. Zuo, M. Fedele, C. Helsens, D. Hill, S. Iguro, and M. Klute, Prospects for B_c^+ and $B^+ \to \tau^+\nu_\tau$ at FCC-ee, Eur. Phys. J. C **84**, 87 (2024).

[132] S. Iguro, Revival of H^- interpretation of $R_{D^{(*)}}$ anomaly and closing low mass window, Phys. Rev. D **105**, 095011 (2022).

[133] M. Blanke, S. Iguro, and H. Zhang, Towards ruling out the charged Higgs interpretation of the $R_{D^{(*)}}$ anomaly, J. High Energy Phys. 06 (2022) 043.

[134] HPQCD Collaboration, $B_c \to J/\psi$ form factors for the full q^2 range from lattice QCD, Phys. Rev. D **102**, 094518 (2020).

[135] T. Yasmeen, I. Ahmed, S. Shafaq, M. Arslan, and M. J. Aslam, Probing new physics in light of recent developments in $b \to c\ell\nu$ transitions, Prog. Theor. Exp. Phys. **2024**, 073B07 (2024).

[136] T. Gutsche, M. A. Ivanov, J. G. Körner, V. E. Lyubovitskij, P. Santorelli, and N. Habyl, Semileptonic decay $\Lambda_b \to \Lambda_c + \tau^- + \overline{\nu_\tau}$ in the covariant confined quark model, Phys. Rev. D **91**, 074001 (2015); **91**, 119907(E) (2015).

[137] S. Shivashankara, W. Wu, and A. Datta, $\Lambda_b \to \Lambda_c\tau\bar{\nu}_\tau$ decay in the standard model and with new physics, Phys. Rev. D **91**, 115003 (2015).

[138] W. Detmold, C. Lehner, and S. Meinel, $\Lambda_b \to p\ell^-\bar{\nu}_\ell$ and $\Lambda_b \to \Lambda_c\ell^-\bar{\nu}_\ell$ form factors from lattice QCD with relativistic heavy quarks, Phys. Rev. D **92**, 034503 (2015).

[139] X.-Q. Li, Y.-D. Yang, and X. Zhang, $\Lambda_b \to \Lambda_c\tau\bar{\nu}_\tau$ decay in scalar and vector leptoquark scenarios, J. High Energy Phys. 02 (2017) 068.

[140] A. Datta, S. Kamali, S. Meinel, and A. Rashed, Phenomenology of $\Lambda_b \to \Lambda_c\tau\bar{\nu}_\tau$ using lattice QCD calculations, J. High Energy Phys. 08 (2017) 131.

[141] F. U. Bernlochner, Z. Ligeti, D. J. Robinson, and W. L. Sutcliffe, Precise predictions for $\Lambda_b \to \Lambda_c$ semileptonic decays, Phys. Rev. D **99**, 055008 (2019).

[142] M. Neubert, Heavy quark symmetry, Phys. Rep. **245**, 259 (1994).

[143] E. Di Salvo, F. Fontanelli, and Z. J. Ajaltouni, Detailed study of the decay $\Lambda_b \to \Lambda_c \tau \bar{\nu}_\tau$, Int. J. Mod. Phys. A **33**, 1850169 (2018).

[144] Q.-Y. Hu, X.-Q. Li, and Y.-D. Yang, $b \to c\tau\nu$ transitions in the standard model effective field theory, Eur. Phys. J. C **79**, 264 (2019).

[145] A. Ray, S. Sahoo, and R. Mohanta, Probing new physics in semileptonic Λ_b decays, Phys. Rev. D **99**, 015015 (2019).

[146] C. Murgui, A. Peñuelas, M. Jung, and A. Pich, Global fit to $b \to c\tau\nu$ transitions, J. High Energy Phys. 09 (2019) 103.

[147] N. Penalva, E. Hernández, and J. Nieves, Further tests of lepton flavour universality from the charged lepton energy distribution in $b \to c$ semileptonic decays: The case of $\Lambda_b \to \Lambda_c \ell \bar{\nu}_\ell$, Phys. Rev. D **100**, 113007 (2019).

[148] M. Ferrillo, A. Mathad, P. Owen, and N. Serra, Probing effects of new physics in $\Lambda_b^0 \to \Lambda_c^+ \mu^- \bar{\nu}_\mu$ decays, J. High Energy Phys. 12 (2019) 148.

[149] X.-L. Mu, Y. Li, Z.-T. Zou, and B. Zhu, Investigation of effects of new physics in $\Lambda_b \to \Lambda_c \tau \bar{\nu}_\tau$ decay, Phys. Rev. D **100**, 113004 (2019).

[150] M. Fedele, M. Blanke, A. Crivellin, S. Iguro, T. Kitahara, U. Nierste, and R. Watanabe, Impact of $\Lambda_b \to \Lambda_c \tau\nu$ measurement on new physics in $b \to c l\nu$ transitions, Phys. Rev. D **107**, 055005 (2023).

[151] LHCb Collaboration, Measurement of the shape of the $\Lambda_b^0 \to \Lambda_c^+ \mu^- \bar{\nu}_\mu$ differential decay rate, Phys. Rev. D **96**, 112005 (2017).

[152] DELPHI Collaboration, Measurement of the Λ_b^0 decay form-factor, Phys. Lett. B **585**, 63 (2004).

[153] CDF Collaboration, First measurement of the ratio of branching fractions $B(\Lambda_b^0 \to \Lambda_c^+ \mu^- \bar{\nu}_\mu)/B(\Lambda_b^0 \to \Lambda_c^+ \pi^-)$, Phys. Rev. D **79**, 032001 (2009).

[154] LHCb Collaboration, Determination of the quark coupling strength $|V_{ub}|$ using baryonic decays, Nat. Phys. **11**, 743 (2015).

[155] LHCb Collaboration, Observation of the decay $\Lambda_b^0 \to \Lambda_c^+ \tau^- \bar{\nu}_\tau$, Phys. Rev. Lett. **128**, 191803 (2022).

[156] F. U. Bernlochner, Z. Ligeti, M. Papucci, and D. J. Robinson, Interpreting LHCb's $\Lambda_b \to \Lambda_c \tau \bar{\nu}$ measurement and puzzles in semileptonic Λ_b decays, Phys. Rev. D **107**, L011502 (2023).

[157] S. Descotes-Genon, L. Hofer, J. Matias, and J. Virto, Global analysis of $b \to s\ell\ell$ anomalies, J. High Energy Phys. 06 (2016) 092.

[158] R.-X. Shi, L.-S. Geng, B. Grinstein, S. Jäger, and J. Martin Camalich, Revisiting the new-physics interpretation of the $b \to c\tau\nu$ data, J. High Energy Phys. 12 (2019) 065.

[159] D. A. Faroughy, A. Greljo, and J. F. Kamenik, Confronting lepton flavor universality violation in B decays with high-p_T tau lepton searches at LHC, Phys. Lett. B **764**, 126 (2017).

[160] S. Iguro, Conclusive probe of the charged Higgs solution of P_5' and $R_{D^{(*)}}$ discrepancies, Phys. Rev. D **107**, 095004 (2023).

[161] M. Tanaka, Charged Higgs effects on exclusive semi-tauonic B decays, Z. Phys. C **67**, 321 (1995).

[162] K. Cheung, W.-Y. Keung, and P.-Y. Tseng, Isodoublet vector leptoquark solution to the muon $g-2$, $R_{K,K*}$, $R_{D,D*}$, and W-mass anomalies, Phys. Rev. D **106**, 015029 (2022).

[163] S. Iguro and Y. Omura, A closer look at isodoublet vector leptoquark solution to the $R_{D^{(*)}}$ anomaly, J. High Energy Phys. 11 (2023) 084.

[164] L. Di Luzio, A. Greljo, and M. Nardecchia, Gauge leptoquark as the origin of B-physics anomalies, Phys. Rev. D **96**, 115011 (2017).

[165] A. Greljo and B. A. Stefanek, Third family quark–lepton unification at the TeV scale, Phys. Lett. B **782**, 131 (2018).

[166] C. Cornella, J. Fuentes-Martin, and G. Isidori, Revisiting the vector leptoquark explanation of the B-physics anomalies, J. High Energy Phys. 07 (2019) 168.

[167] L. Di Luzio, J. Fuentes-Martin, A. Greljo, M. Nardecchia, and S. Renner, Maximal flavour violation: A Cabibbo mechanism for leptoquarks, J. High Energy Phys. 11 (2018) 081.

[168] M. Bordone, C. Cornella, J. Fuentes-Martin, and G. Isidori, A three-site gauge model for flavor hierarchies and flavor anomalies, Phys. Lett. B **779**, 317 (2018).

[169] M. Bordone, C. Cornella, J. Fuentes-Martín, and G. Isidori, Low-energy signatures of the PS^3 model: From B-physics anomalies to LFV, J. High Energy Phys. 10 (2018) 148.

[170] M. Blanke and A. Crivellin, B meson anomalies in a Pati-Salam model within the Randall-Sundrum background, Phys. Rev. Lett. **121**, 011801 (2018).

[171] S. Balaji, R. Foot, and M. A. Schmidt, Chiral SU(4) explanation of the $b \to s$ anomalies, Phys. Rev. D **99**, 015029 (2019).

[172] S. Balaji and M. A. Schmidt, Unified SU(4) theory for the $R_{D^{(*)}}$ and $R_{K^{(*)}}$ anomalies, Phys. Rev. D **101**, 015026 (2020).

[173] J. Fuentes-Martín and P. Stangl, Third-family quark-lepton unification with a fundamental composite Higgs, Phys. Lett. B **811**, 135953 (2020).

[174] J. Fuentes-Martín, G. Isidori, M. König, and N. Selimović, Vector leptoquarks beyond tree level III: Vector-like fermions and flavor-changing transitions, Phys. Rev. D **102**, 115015 (2020).

[175] D. Guadagnoli, M. Reboud, and P. Stangl, The dark side of 4321, J. High Energy Phys. 10 (2020) 084.

[176] M. J. Dolan, T. P. Dutka, and R. R. Volkas, Lowering the scale of Pati-Salam breaking through seesaw mixing, J. High Energy Phys. 05 (2021) 199.

[177] S. F. King, Twin Pati-Salam theory of flavour with a TeV scale vector leptoquark, J. High Energy Phys. 11 (2021) 161.

[178] S. Iguro, J. Kawamura, S. Okawa, and Y. Omura, TeV-scale vector leptoquark from Pati-Salam unification with vectorlike families, Phys. Rev. D **104**, 075008 (2021).

[179] S. Iguro, J. Kawamura, S. Okawa, and Y. Omura, Importance of vector leptoquark-scalar box diagrams in Pati-Salam unification with vector-like families, J. High Energy Phys. 07 (2022) 022.

[180] J. Heeck and D. Teresi, Pati-Salam explanations of the B-meson anomalies, J. High Energy Phys. 12 (2018) 103.

[181] D. Marzocca, Addressing the B-physics anomalies in a fundamental composite Higgs model, J. High Energy Phys. 07 (2018) 121.

[182] D. Marzocca and S. Trifinopoulos, Minimal explanation of flavor anomalies: B-meson decays, muon magnetic mo-

ment, and the Cabibbo angle, Phys. Rev. Lett. **127**, 061803 (2021).
[183] D. Bečirević, I. Doršner, S. Fajfer, D. A. Faroughy, N. Košnik, and O. Sumensari, Scalar leptoquarks from grand unified theories to accommodate the B-physics anomalies, Phys. Rev. D **98**, 055003 (2018).
[184] K. S. Babu, P. S. B. Dev, S. Jana, and A. Thapa, Unified framework for B-anomalies, muon $g-2$ and neutrino masses, J. High Energy Phys. 03 (2021) 179.
[185] T. Faber, M. Hudec, M. Malinský, P. Meinzinger, W. Porod, and F. Staub, A unified leptoquark model confronted with lepton non-universality in B-meson decays, Phys. Lett. B **787**, 159 (2018).
[186] T. Faber, Y. Liu, W. Porod, M. Hudec, M. Malinský, F. Staub, and H. Kolešová, Collider phenomenology of a unified leptoquark model, Phys. Rev. D **101**, 095024 (2020).
[187] L. Di Luzio, M. Kirk, A. Lenz, and T. Rauh, ΔM_s theory precision confronts flavour anomalies, J. High Energy Phys. 12 (2019) 009.
[188] L. Calibbi, A. Crivellin, and T. Li, Model of vector leptoquarks in view of the B-physics anomalies, Phys. Rev. D **98**, 115002 (2018).
[189] A. Crivellin, D. Müller, and F. Saturnino, Flavor phenomenology of the leptoquark singlet-triplet model, J. High Energy Phys. 06 (2020) 020.
[190] CMS Collaboration, Search for pair-produced vector-like leptons in final states with third-generation leptons and at least three b quark jets in proton-proton collisions at $s = 13$ TeV, Phys. Lett. B **846**, 137713 (2023).
[191] CMS Collaboration, Review of searches for vector-like quarks, vector-like leptons, and heavy neutral leptons in proton-proton collisions at $\sqrt{s} = 13$ TeV at the CMS experiment, arXiv:2405.17605.
[192] ATLAS Collaboration, Search for third-generation vector-like leptons in pp collisions at $\sqrt{s} = 13$ TeV with the ATLAS detector, J. High Energy Phys. 07 (2023) 118.
[193] CMS Collaboration, Search for heavy neutrinos and third-generation leptoquarks in hadronic states of two τ leptons and two jets in proton-proton collisions at $\sqrt{s} = 13$ TeV, J. High Energy Phys. 03 (2019) 170.
[194] ATLAS Collaboration, Searches for third-generation scalar leptoquarks in $\sqrt{s} = 13$ TeV pp collisions with the ATLAS detector, J. High Energy Phys. 06 (2019) 144.
[195] ATLAS Collaboration, Search for pair production of third-generation scalar leptoquarks decaying into a top quark and a τ-lepton in pp collisions at $\sqrt{s} = 13$ TeV with the ATLAS detector, J. High Energy Phys. 06 (2021) 179.
[196] E. E. Jenkins, A. V. Manohar, and M. Trott, Renormalization group evolution of the standard model dimension six operators II: Yukawa dependence, J. High Energy Phys. 01 (2014) 035.
[197] R. Alonso, E. E. Jenkins, A. V. Manohar, and M. Trott, Renormalization group evolution of the standard model dimension six operators III: Gauge coupling dependence and phenomenology, J. High Energy Phys. 04 (2014) 159.
[198] M. González-Alonso, J. Martin Camalich, and K. Mimouni, Renormalization-group evolution of new physics contributions to (semi)leptonic meson decays, Phys. Lett. B **772**, 777 (2017).
[199] J. Aebischer, A. Crivellin, and C. Greub, QCD improved matching for semileptonic B decays with leptoquarks, Phys. Rev. D **99**, 055002 (2019).
[200] A. Crivellin, J. F. Eguren, and J. Virto, Next-to-leading-order QCD matching for $\Delta F = 2$ processes in scalar leptoquark models, J. High Energy Phys. 03 (2022) 185.
[201] R. Barbieri, G. R. Dvali, and L. J. Hall, Predictions from a U(2) flavor symmetry in supersymmetric theories, Phys. Lett. B **377**, 76 (1996).
[202] R. Barbieri, L. J. Hall, and A. Romanino, Consequences of a U(2) flavor symmetry, Phys. Lett. B **401**, 47 (1997).
[203] R. Barbieri, G. Isidori, J. Jones-Perez, P. Lodone, and D. M. Straub, $U(2)$ and minimal flavour violation in supersymmetry, Eur. Phys. J. C **71**, 1725 (2011).
[204] R. Barbieri, P. Campli, G. Isidori, F. Sala, and D. M. Straub, B-decay CP-asymmetries in SUSY with a $U(2)^3$ flavour symmetry, Eur. Phys. J. C **71**, 1812 (2011).
[205] R. Barbieri, D. Buttazzo, F. Sala, and D. M. Straub, Flavour physics from an approximate $U(2)^3$ symmetry, J. High Energy Phys. 07 (2012) 181.
[206] G. Blankenburg, G. Isidori, and J. Jones-Perez, Neutrino masses and LFV from minimal breaking of $U(3)^5$ and $U(2)^5$ flavor symmetries, Eur. Phys. J. C **72**, 2126 (2012).
[207] R. Barbieri, G. Isidori, A. Pattori, and F. Senia, Anomalies in B-decays and $U(2)$ flavour symmetry, Eur. Phys. J. C **76**, 67 (2016).
[208] J. Fuentes-Martín, G. Isidori, J. Pagès, and K. Yamamoto, With or without U(2)? Probing non-standard flavor and helicity structures in semileptonic B decays, Phys. Lett. B **800**, 135080 (2020).
[209] M. Fernández Navarro and S. F. King, B-anomalies in a twin Pati-Salam theory of flavour including the 2022 LHCb $R_{K^{(*)}}$ analysis, J. High Energy Phys. 02 (2023) 188.
[210] S. Iguro and T. Kitahara, Electric dipole moments as probes of B anomaly, arXiv:2307.11751.
[211] A. Crivellin, C. Greub, D. Müller, and F. Saturnino, Importance of loop effects in explaining the accumulated evidence for new physics in B decays with a vector leptoquark, Phys. Rev. Lett. **122**, 011805 (2019).
[212] C. H. García-Duque, J. H. Muñoz, N. Quintero, and E. Rojas, Extra gauge bosons and lepton flavor universality violation in Υ and B meson decays, Phys. Rev. D **103**, 073003 (2021).
[213] C. H. García-Duque, J. M. Cabarcas, J. H. Muñoz, N. Quintero, and E. Rojas, Singlet vector leptoquark model facing recent LHCb and *BABAR* measurements, Nucl. Phys. **B988**, 116115 (2023).
[214] S. Descotes-Genon, S. Fajfer, J. F. Kamenik, and M. Novoa-Brunet, Testing lepton flavor universality in $\Upsilon(4S)$ decays, Phys. Rev. D **103**, 113009 (2021).
[215] M. Beneke, Y. Kiyo, P. Marquard, A. Penin, J. Piclum, D. Seidel, and M. Steinhauser, Leptonic decay of the $\Upsilon(1S)$ meson at third order in QCD, Phys. Rev. Lett. **112**, 151801 (2014).
[216] CLEO Collaboration, First observation of $\Upsilon(3S) \to \tau^+\tau^-$ and tests of lepton universality in upsilon decays, Phys. Rev. Lett. **98**, 052002 (2007).

[217] R. Van Royen and V. F. Weisskopf, Hadron decay processes and the quark model, Nuovo Cimento Soc. Ital. Fis. **50A**, 617 (1967); **51A**, 583(E) (1967).
[218] D. Y. Bardin and G. Passarino, *The Standard Model in the Making: Precision Study of the Electroweak Interactions* (Clarendon Press, Oxford, 1999).
[219] S. Matsuzaki, K. Nishiwaki, and K. Yamamoto, Simultaneous interpretation of K and B anomalies in terms of chiral-flavorful vectors, J. High Energy Phys. 11 (2018) 164.
[220] L. Allwicher, D. A. Faroughy, F. Jaffredo, O. Sumensari, and F. Wilsch, HighPT: A tool for High-PT Drell-Yan tails beyond the standard model, Comput. Phys. Commun. **289**, 108749 (2023).
[221] A. Ishikawa (private communication).
[222] W. Buchmuller, R. Ruckl, and D. Wyler, Leptoquarks in lepton—quark collisions, Phys. Lett. B **191**, 442 (1987); **448**, 320(E) (1999).
[223] A. Angelescu, D. Bečirević, D. A. Faroughy, and O. Sumensari, Closing the window on single leptoquark solutions to the B-physics anomalies, J. High Energy Phys. 10 (2018) 183.